

Environmental effects in stellar mass gravitational wave sources I: Expected fraction of signals with significant dephasing in the dynamical and AGN channels.

Lorenz Zwick^{1,*}, János Takátsy¹, Pankaj Saini¹, Kai Hendriks¹, Johan Samsing¹, Christopher Tiede¹, Connor Rowan¹, and Alessandro A. Trani^{1,2}

¹*Niels Bohr International Academy, The Niels Bohr Institute,
Blegdamsvej 17, DK-2100, Copenhagen, Denmark*

²*National Institute for Nuclear Physics – INFN, Sezione di Trieste, I-34127, Trieste, Italy*

(Dated: April 1, 2025)

We present the first overview of the expected quantity of signals which will showcase significant gravitational wave phase shifts caused by astrophysical environments, considering the upcoming A+ and A# LIGO/Virgo/KAGRA, Cosmic Explorer and Einstein Telescope detectors. We construct and analyse two general families of dephasing prescriptions with extensions to eccentric sources, as well as collect five specific prescriptions for the fundamental smoking gun physical mechanisms at play in the dynamical and AGN formation channel for stellar mass binary black holes: Roemer delays, tidal forces and hydrodynamical interactions. We compute the expected fraction of signals containing astrophysical dephasing, as a function of environmental properties and based on observed distributions of binary parameters. We find that next generation detectors can expect to find environmental effects in hundreds of detected signals.

I. INTRODUCTION

Almost a decade after the first detection of gravitational waves (GWs), many fundamental aspects of binary black hole (BBH) astrophysics remain unanswered: Where are binaries preferentially formed? Which astrophysical mechanisms shape observable binary properties? How do such mechanisms couple to in-spiralling GW sources? In the current framework of population based hierarchical inference, properties of many observed GW sources are aggregated and analysed statistically in order to produce constraints on their astrophysical formation pathways [1–10]. However, despite the increasing number of signals in the LIGO-Virgo-KAGRA (LVK) catalogue, progress is proving to be challenging, as smoking gun features from different environments are hard to distinguish from intrinsic variability of black hole (BH) binary properties [7]. In recent years, two pathways have emerged to overcome the limitations of population based statistics, which focus instead on extract astrophysical information from a small number of GW signals. The first is the study of eccentricity as a smoking gun signature of dynamical formation channels [e.g. 11–25], which is becoming more and more relevant as the low-frequency sensitivity of ground based detector improves [26–29]. The second is more elusive, though perhaps hides even more potential: it is the study of so called “Environmental Effects” (EE).

EEs refer to small deviations from an expected vacuum waveform, caused by astrophysical perturbations to the GW source’s dynamics [30–58]. The most studied type of EE in GWs consists of a phase-shift, or dephasing, between the vacuum waveform and the perturbed waveform. Dephasing has typically only been considered to be realistically detectable in extreme-mass-ratio inspirals in

the milli-Hz band, due to the large number of available GW cycles [see e.g. 59, 60]. However, with the advent of third generation GW detectors it is worth to reconsider whether dephasing may arise in stellar mass binary black holes, as a natural consequence of both the dynamical and the AGN formation channel. In the former, Roemer delays [37, 61–64] and tidal fields [49, 65–68] due to third bodies affect the observed GW frequency and the inspiral rate of binaries. In the latter, gas accretion and drag [33, 45, 56, 69, 70] will similarly induce modifications to the secular evolution of binary orbital parameters.

Despite the existence of many physical mechanisms that induce GW phase shifts, it is still unclear which have realistic prospects for detection, and which regions of binary parameter space are most likely to showcase potentially detectable EEs. While a number of individual studies on the detectability of de-phasing exist, no work has collected and directly compared their relevance for stellar mass binary sources in light of near future ground based detectors. Furthermore, the interaction between environmentally caused de-phasing and eccentricity is largely unexplored (with the exception e.g. promising work on Roemer delays in [61], and on extreme mass ratio systems in [70]). This aspect is crucial, as eccentricity is itself considered a smoking gun signature of more complex BH binary formation channels [see e.g. 71–77], and it strongly affects both the GW emission of binaries [78] and their coupling to external forces. As the sensitivity of ground based detectors improves, it is therefore of great importance to revisit the topic of EE and its interaction with eccentricity in order to prepare appropriate waveform models that can extract the maximal amount of astrophysical information from GW signals (see Fig. 1 for an illustration of this principle).

In this work we present an overview of the significance and detectability of dephasing in stellar mass BBHs, which are most likely to arise in both the dynamical [16, 19, 24, 79–99] and AGN channel [74, 100–106]. We

* lorenz.zwick@nbi.ku.dk

construct two families of dephasing prescriptions that have characteristic extensions to high eccentricities, and thoroughly discuss their properties in terms of detectability. Then, we collect or develop five dephasing prescriptions which specifically model smoking gun physical mechanisms at play in the aforementioned formation channels, focusing on Roemer delays, tidal forces and various type of hydrodynamical interactions with a gaseous medium. We analyse their expected magnitude and detectability considering four different near future ground-based detector configurations, i.e LVK A+ [107, 108] and A# [109] sensitivities, Cosmic Explorer [110] and the Einstein Telescope [111], for sources with a small but non-vanishing eccentricity. Furthermore, we briefly comment on the detectability of such EE in LISA. We then estimate the expected fractions of sources with significant environmental dephasing based on currently observed BH binary parameter distributions, providing an expectation as a function of the parameters of the environment. Our results provide a first estimate of the expected fraction of signals containing EEs in ground based GW detectors, based on observed population distribution. They can be used to guide further development of EE models and waveforms containing dephasing prescriptions. An extension of this work to highly eccentric sources is left for paper II.

The paper is structured as follows: In section II we explain the methodology used to model gravitational waveforms and gravitational wave sources, including a criterion to define significant GW perturbations. In section III, we derive and discuss the properties of a set of general dephasing prescriptions and their extensions to higher eccentricity. In section IV we collect or derive explicit dephasing prescriptions for expected EE in the dynamical and AGN formation channels. In V we present the results for the expected detectability fractions of the EE as a function of the environmental parameters. We summarise the results and present some concluding remarks in section VI.

II. METHODOLOGY

A. Dephasing SNR criteria

The purpose of this work is to extensively survey the parameter space of stellar mass BH binaries in order to identify regions in which EE are likely to be present. In particular we want to finely sample source redshift z , rest-frame chirp mass \mathcal{M} , reduced mass μ and eccentricity e , as well as any parameters required to describe the binary's environment. We require an efficient method to estimate the relevance of environmentally caused GW perturbations given the properties of the source, environment, and a GW detector. Therefore we employ the δSNR criterion [see e.g. 34, 49], which states that a waveform perturbation is significant if the following inequality

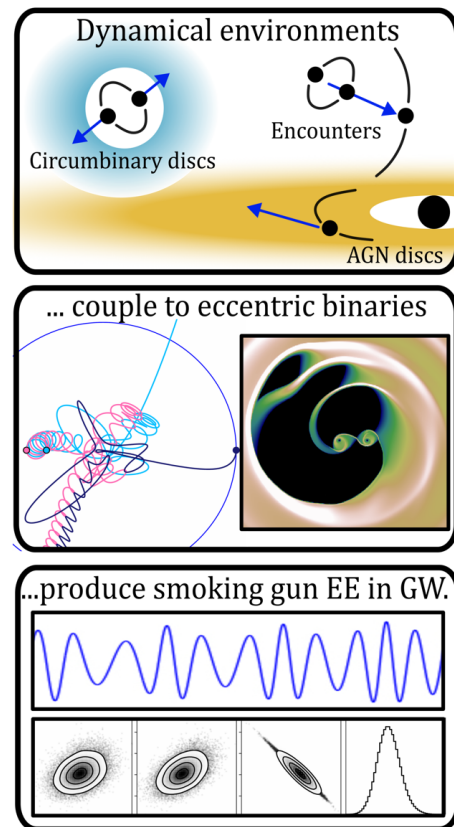


FIG. 1. Illustration of the motivating principles for this work. Identifying and inferring eccentricity and/or environmental perturbations in individual binary sources of GW can reveal smoking gun signatures of binary environments.

is satisfied:

$$\delta\text{SNR}^2 \equiv \langle \Delta h, \Delta h \rangle > \mathcal{C}^2, \quad (1)$$

$$\Delta h = h_{\text{vac}} - h_{\text{EE}} \quad (2)$$

where h_{vac} is the unperturbed vacuum waveform and h_{EE} is the perturbed waveform including EE, and \mathcal{C} is threshold commonly chosen to be $\mathcal{O}(10)$. An example of a reference waveform and the waveform difference Δh can be seen in Fig. 2, compared to the sensitivity of ground based detectors. The inner product $\langle \cdot, \cdot \rangle$ represents the noise weighted SNR of a waveform h :

$$\langle h_1, h_2 \rangle = 2 \int_0^\infty \frac{\tilde{h}_1 \tilde{h}_2^* + \tilde{h}_1^* \tilde{h}_2}{S_n(f')} df' \quad (3)$$

where \tilde{h}_i is the Fourier frequency space representation of the waveform h_i and S_n is the noise power spectral density of a given detector.

The interpretation of Eq. (1) is that the SNR of the difference between unperturbed and perturbed waveforms should reach a certain threshold in order to be significant. In many works, the value of \mathcal{C} is chosen to be 8, in analogy to the typical minimum SNR required for a

confident detection in LVK, accounting for various statistical considerations such as the false-positive rate and the “look-elsewhere effect” [112]. However, given that EE can only ever be detectable on high SNR signals which have already been identified, it is possible that the actual required threshold is lower than the typical value of $\delta\text{SNR} = 8$. In reality, the actual value depends on the employed waveforms, the detector properties and the specific form of the EE in question.

Satisfying Eq. 1 does not assure that a perturbation may be distinguished in the full parameter estimation procedure, due to the presence of degeneracies. Nevertheless, in this work we will employ a threshold of $\mathcal{C} = 3$ to indicate the presence of significant dephasing, as it is still an indication that the perturbation may be distinguishable in some favourable cases, or introduce some biases in the inference of vacuum parameters. Leaving the problem of degeneracies aside, the δSNR criterion suffices for the purposes of this work, as it indicates whether a waveform perturbation is in principle large enough to result in the presence of significant residual power when the best fit vacuum model is removed. We note that further work is required to go from the criterion suggested by Eq. 1 to the full parameter estimation problem. However, preliminary work on distinguishing EE in a Bayesian context exists and is promising [e.g. 46, 55, 69, 113, 114]

B. Vacuum waveform model

The expected GW signal from a Newtonian inspiralling binary is determined by the following parameters:

$$\text{Vac. par.} := \begin{cases} z; & \text{Redshift} \\ \mathcal{M}; & \text{Chirp mass} \\ \mu; & \text{Reduced mass} \\ e(f_0); & \text{eccentricity at } f_0 \end{cases} \quad (4)$$

where f_0 is a reference frequency and we neglected binary spins, and averaged over orientation and sky localisation. Additionally, EE will be typically parameterised by a single additional free parameter ξ . After extensive testing, we find that satisfactory resolution for this work, which considers four detector sensitivities and five types of environmental effect, requires the evaluation of the δSNR criterion for approximately 10^8 waveforms. Therefore, we are limited to using extremely efficient waveforms that can be evaluated precisely in Eq. 1 in a time of order few ms. This completely excludes the possibility of estimating detectability with more sophisticated methods such as parameter inference with e.g. Monte-Carlo Markov-Chain pipelines.

Here we employ a modification to the well known analytical Newtonian waveform result in the stationary phase approximation, which for circular binaries reads

[115, 116]:

$$\tilde{h}(f) = \frac{Q}{D(z)} \left(\frac{G\mathcal{M}_z}{c^3} \right)^{5/6} f^{-7/6} \exp[i(-\psi_{\text{vac}})], \quad (5)$$

where f is the observer frame GW frequency of the fundamental mode, \mathcal{M}_z is the red-shifted chirp mass, $D(z)$ is the luminosity distance, $Q = 2/5$ is a geometric prefactor that accounts for projections of the wave onto an L-shaped interferometric detector in the long wavelength limit [117]. The Fourier domain phase ψ_{vac} is given by:

$$\psi_{\text{vac}} = -\frac{\pi}{4} - \frac{3}{4} (8\pi\mathcal{M}_z f)^{-5/3}, \quad (6)$$

where we neglected a constant phase offset ϕ_c and an integration constant t_c representing the phase and time at coalescence, as they do not influence the δSNR results.

To adapt Eq. 5 to low eccentricities, we note that $\tilde{h}(f)^2 = 2T_{\text{in}}f \times S_{\text{GW}}(f)$, where $S_{\text{GW}}(f)$ is the GW’s power spectral density and T_{in} is the binary’s in-spiral timescale [78, 118, 119]. For $e \lesssim 0.2$, we can assume that the majority of the orbital binding energy is radiated in the fundamental GW mode at twice the orbital frequency, i.e. $f = 2\Omega_{\text{K}}/(1+z)$, where Ω_{K} is the binary’s orbital frequency in the rest frame. Then, the only effect of eccentricity is to reduce the inspiral timescale, which causes the radiated power to be suppressed for higher eccentricities:

$$\tilde{h}(f) = \tilde{h}(f)^{e=0} \times \sqrt{\frac{\dot{f}_{e=0}}{\dot{f}(e)}}. \quad (7)$$

Note that the phase of the GW is also modified by eccentricity. In the small eccentricity limit, the phase can be decomposed into circular part and eccentric corrections [120].

$$\psi_{\text{vac}} = \psi_{\text{vac}}^{e=0} + \Delta\psi^{\text{ecc}}(f, e^2). \quad (8)$$

However, this aspect is irrelevant in our δSNR calculations as we are looking at differences in phases, and the vacuum phase evolution is subtracted away. We note that here, and for the remainder of our paper, the eccentricity e specifically denotes the value of the binary’s eccentricity at a given fundamental GW frequency f . For the eccentricity evolution, we use the following fit, adapted from [121]:

$$e(f) \approx \frac{16.83 - 3.814b(f)^{0.3858}}{16.04 + 8.1b(f)^{1.637}} \quad (9)$$

$$b(f) = \left(\frac{f}{f_0} \right)^{2/3} \frac{(1 + \frac{121}{304}e_0^2)^{870/2299}}{1 - e_0^2} e_0^{12/19}, \quad (10)$$

where e_0 is the eccentricity at a reference frequency f_0 . We note again that the adopted modelling of eccentricity in this paper is only appropriate for small values, and that a more thorough analysis of eccentric sources will be performed in paper II. In this regime, the majority

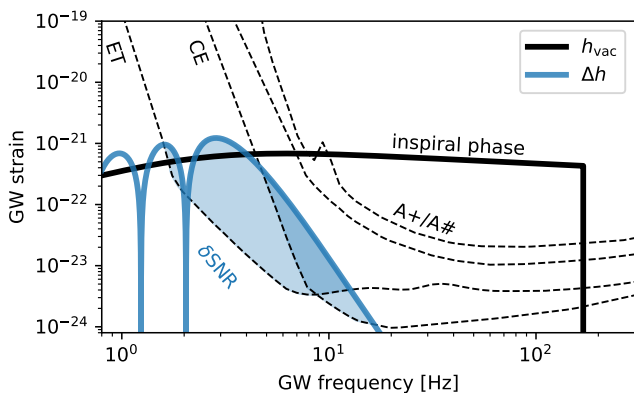


FIG. 2. The inspiral phase characteristic strain h_{vac} of a $20 M_{\odot}$, equal mass binary source at $z = 0.3$ (black line), according to our waveform model (see Eqs. 5 and 7). The binary has a reference eccentricity of $e_{10 \text{ Hz}} = 0.1$. Note how the radiated power at lower frequencies is suppressed due to eccentricity. The blue line denotes the the residual Δh between h_{vac} and a phase shifted GW where strong Roemer delays are present (see Eq. 43). The strains are compared to the sensitivities of near future ground based detectors, where the shaded blue areas denote the available δSNR of the signal (Eq. 1).

of energy is radiated in the fundamental GW mode at twice the orbital frequency. In fact, Newtonian waveforms of the form shown in Eq. 5 typically give a slightly conservative estimate of the optimal SNR for binaries as they do not account for the additional energy radiated via higher order harmonics and post-Newtonian fluxes [121]. Additionally, higher modes caused by the presence of eccentricity may enter the band of a given detector while the binary is orbiting at lower frequencies, which can lead to higher overall SNRs [121]. Furthermore, in terms of δSNR results for phase shifted waveforms, the precise form of the vacuum waveform does not affect our results beyond providing a slightly different overall SNR normalisation, i.e. $= \langle h_{\text{vac}}, h_{\text{vac}} \rangle$.

It is crucial to state that a complete analysis of the extensions of de-phasing prescriptions to $e \sim 0.2$ and above do in fact require eccentric waveforms, for the following two reasons. Firstly, dephasing will accumulate faster in the phase of higher order GW modes since they scale with multiples of the binary orbital frequency. Secondly, highly eccentric binaries may enter the band of a given detector at comparatively large separations (lower orbital frequencies), where EE are typically stronger. The effect of including higher order eccentric harmonics on the δSNR of dephasing is highly interesting and will be the subject of paper II.

C. Binary population

In this work, we wish to estimate the fraction of sources which will present a significant dephasing depending on a choice of detector, environmental properties and binary

parameters. For this reason, we require estimates for the distributions of intrinsic binary parameters over which we can marginalise δSNR results. As mentioned in the introduction, the determination of the intrinsic distributions of BH binary parameters is a great achievement of the current LVK instruments. It is the current understanding that the observed distributions emerge as a combination of a small number of distinct binary formation pathways, most commonly separated into the isolated, dynamical and AGN binary formation channels [see e.g. 8]¹. A significant amount of population synthesis works have produced estimates of the expected rates of detectable GW signals originating from these channels, often resulting in rates comparable with the overall LVK detections. However, disentangling the individual contribution of each formation channel within the data remains a challenge, and many conflicting claims exist in the literature.

For the purposes of this work, we make the following simplifying assumptions regarding the distribution of binary parameters. Firstly, we assume that the overall observed LVK distributions in binary mass, mass ratio and redshift is representative of any given formation channel that showcases a certain EE. Then, our results for the expected detection rates for different EE can be adjusted by simply multiplying the total detection fraction with an efficiency parameter ϵ that accounts for the fraction of sources that originate from that particular channel. Secondly, we assume that the distributions for the parameters are independent of each other, i.e.:

$$\mathcal{P}(z|\mathcal{M}|\mu|e) \sim \mathcal{P}(z)\mathcal{P}(\mathcal{M})\mathcal{P}(\mu)\mathcal{P}(e), \quad (11)$$

where $\mathcal{P}(x)$ is the probability of finding a binary with parameters x . While both of these assumptions are most likely inaccurate, they serve as a first order approximation to compute expectations for the detectability of dephasing within the rather large uncertainty of the properties of binary environments. The distributions of intrinsic binary properties are taken from [124], and plotted in Fig. 3. Here we make the standard identification $\mathcal{P}(x) \sim dR/dx$, where R is the binary merger rate as reconstructed from LVK observations. Note that here we are referring to the intrinsic binary merger rate rather than the observed one.

In this particular work, we do not perform an extensive analysis of the variation of the detection fractions as a function of the population parameter distributions. Instead, we base the results on the observed LVK binary merger rates. Since the eccentricity distributions are still unconstrained, we simply assume a half-Gaussian PDF between 0 and 0.2 for the binary eccentricity. We can then vary the standard deviation σ_e to model more or

¹ Other pathways such as the primordial BH formation channel may also contribute to the detected rates [122, 123]

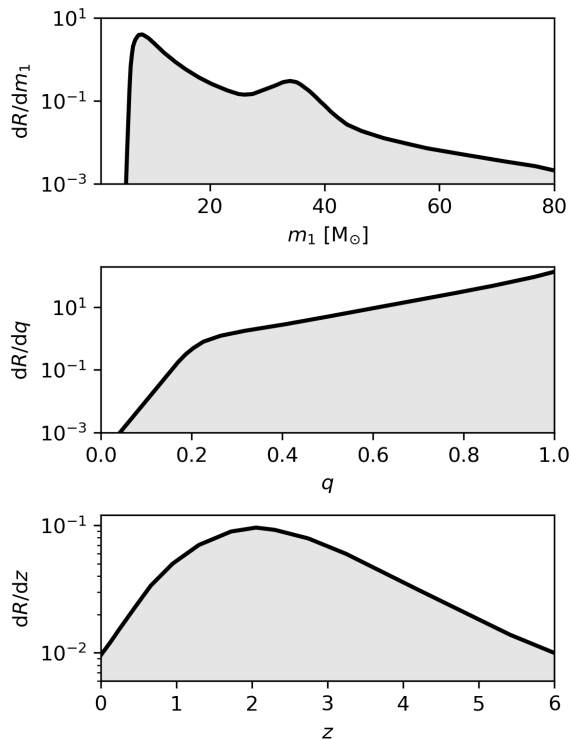


FIG. 3. Differential merger rates R of BH binaries with primary mass m_1 , mass ratio q at redshift z . The panels above are reconstructions of the third LVK observation run [124]. The distribution in redshift is extended by extrapolating with a simple fit of the observed star formation rate [128, 129].

less eccentric binary populations:

$$\mathcal{P}(e(f_0)) \sim \exp\left(-\frac{e(f_0)^2}{2\sigma_e^2}\right). \quad (12)$$

Our baseline choice will be $\sigma_e = 0.01$, as it is lower than the currently estimated limit of detectability for LVK [125, 126], and there are only potential signs of eccentricity in a small number of detected sources [127]. Another sensible choice for the eccentricity distribution is a log-normal distribution with ~ -2 as the mean and a standard deviation 1 dex. We note here that neither of these represents the eccentricity distribution of the underlying populations. Here we only consider a choice of $\mathcal{P}(e)$ as a baseline and find that eccentricity distribution plays a minor role in determining the detectability of EE at this level of analysis. We reserve a more thorough treatment of eccentricity distributions for paper II, in which we also consider proper eccentric waveforms. Secondly, we perform tests in which we vary the SNR threshold required to consider a GW source to be detectable. The implications of varying this parameter are discussed in section V.

III. GENERAL DE-PHASING PRESCRIPTIONS

A. De-phasing families

GW dephasing can arise in a wide range of astrophysical scenarios. Despite the large variety, we can collect the vast majority of cases into three distinct mechanisms (see [35] for a review of EE in small mass ratio systems, (and the upcoming Takatsy et al. 2025 for an extensive first principles derivation of the properties of phase shifts). The first is through direct perturbations to the sources inspiral rate $\dot{f} \rightarrow \dot{f}_{\text{vac}} + \delta\dot{f}$, such that:

$$\delta\phi \sim \int \int (\delta\dot{f} dt) dt \sim \frac{1}{2}\delta\dot{f} \times T_{\text{obs}}^2, \quad (13)$$

where $\delta\phi$ is the GW dephasing in the time domain, and T_{obs} is the observation time. Note that here we used a almost-monochromatic approximation where $\delta\dot{f}$ is constant. This is often appropriate as de-phasing tends to accumulate primarily in the very early inspiral phases of binary evolution.

The second mechanism is through the accumulation of a time dependent Doppler shift $\delta f \sim v/c$, where v is the line of sight velocity and c is the speed of light. While one would expect de-phasing of the form:

$$\delta\phi \sim \int v/c dt \sim \delta f \times T_{\text{obs}}, \quad (14)$$

a constant Doppler shift is fully degenerate with the binary's source mass². Therefore, the significant de-phasing due to Doppler shifts is more appropriately defined as the one accumulating through the source acceleration, rather than velocity [see e.g. 37, 133]:

$$\delta\phi \sim \int \left(\int \dot{v}/c dt \right) dt \sim \frac{1}{2}\delta\dot{f} \times T_{\text{obs}}^2. \quad (15)$$

Despite the different origin, this effect reduces to the same scaling with the inspiral timescale as in Eq. 13.

The third type of mechanism to produce de-phasing occurs whenever some external potential causes the binary's binding energy to be modified $E_B \rightarrow E_B + \delta E$, while the in-spiral rate remains unaffected [35, 49]. Then, the additional binding energy requires time to be radiated away, producing a change in the in-spiral timescale $\delta T/T_{\text{in}} \sim \delta E/E_b$. The total phase ϕ_{tot} of the binary is then modified to:

$$\phi_{\text{tot}} = \int_0^{T_{\text{obs}} + \delta T} f dt, \quad (16)$$

² This limitation may be overcome in the case where multiple de-phased images of the same source are present, such as the case with strongly lensed GW sources [130–132].

which implies that the de-phasing scales linearly with the inspiral timescale, which for chirping binaries is the limiting factor in the observation, $T_{\text{obs}} \rightarrow T_{\text{in}}$:

$$\delta\phi \sim f T_{\text{in}} \times \delta E/E_{\text{b}}. \quad (17)$$

Note here that de-phasing due to constant Doppler-shifts also shares this linear scaling in the in-spiral timescale.

Here we propose a general parametrisation for these various mechanisms of de-phasing in a vein similar to [41]. The parametrisation is additionally categorised into two families of functions, each with a distinct extensions to moderate eccentricities, though these will be discussed in more detail in paper II. First, recall that the quantities $\delta\dot{f}$ and δE encode information regarding the coupling between the binary and its environment. In general, they are functions of a time variable t , as well as the binary and environmental parameters. In this work, we only treat orbit averaged quantities (see [134] and also [55] for an initial treatment of non-orbit averaged environmental effects), such that $\delta\dot{f} = \delta\dot{f}(\xi|f, e, \mathcal{M}, \mu)$ and $\delta E = \delta E(\xi|f, e, \mathcal{M}, \mu)$, where once again ξ is the parameter (or set of parameters) describing the environment.

Recall the inspiral rate of a binary emitting GW at an observer frame frequency f :

$$\dot{f}_{\text{vac}} = \frac{96}{5} \pi^{8/3} \left(\frac{G\mathcal{M}_z}{c^3} \right)^{5/3} f^{11/3} \times F(e), \quad (18)$$

where:

$$F(e) = \left(1 + \frac{73}{24}e^2 + \frac{37}{96}e^4 \right) (1 - e^2)^{-7/2}. \quad (19)$$

The resulting GW driven inspiral timescale T_{in} does not have an explicit analytical solution valid for all initial eccentricities, and several approximation schemes have been proposed. Here we adopt the following approximation from [135, 136]:

$$T_{\text{in}} \approx T_{\text{in}}|_{e=0} \times F(e)^{-1} \times R(e) \quad (20)$$

where $T_{\text{in}}|_{e=0}$ is Peters' timescale for circular orbits and the factor $R(e) = 8^{1-\sqrt{1-e}}$ approximates the effect of consistently evolving eccentricity and semimajor axis. Combining the latter equations with the two scalings suggested by Eqs. 13 and 17, we propose two de-phasing families of the form:

$$\delta\phi_{i,j,k;n}^I(f) = \mathcal{A} \times \mathcal{M}^i \mu^j f^n \mathcal{F}_k^I(e), \quad (21)$$

$$\delta\phi_{i,j,k;n}^{II}(f) = \mathcal{A} \times \mathcal{M}^i \mu^j f^n \mathcal{F}_k^{II}(e), \quad (22)$$

where:

$$\mathcal{F}_k^I(e) = e^k \left(\frac{T_{\text{in}}}{T_{\text{in}}^{e=0}} \right)^2 \approx e^k \left(\frac{R(e)}{F(e)} \right)^2 \quad (23)$$

$$\mathcal{F}_k^{II}(e) = e^k \left(\frac{T_{\text{in}}}{T_{\text{in}}^{e=0}} \right) \approx e^k \left(\frac{R(e)}{F(e)} \right). \quad (24)$$

These two families encode all possible scalings of dephasing prescriptions with binary parameters, provided that the quantities $\delta\dot{f}$ and δE are power-laws in f , \mathcal{M} , and are polynomial in e . Crucially, this is typically the case for all current models of astrophysical EEs in the orbit averaged limit.

The eccentricity scaling of these de-phasing families is a mostly novel aspect that requires further discussion. Here we simply comment that if $k = 0$ the functions \mathcal{F}_k^I and \mathcal{F}_k^{II} limit to the value 1 for small e , and the dephasing prescriptions approach the simple power laws that describe the circular case. This is the typical case for EE and for all of the specific prescriptions analysed in this work. The behavior of the prescriptions for other values of k and the existence of related EE will be discussed in detail in paper II. Finally, we note that the conversion from the GW dephasing $\delta\phi$ to the Fourier domain dephasing $\delta\psi$ appropriate for Eq. 1 is not always trivial, in particular in the presence of a time variable eccentricity [see e.g. 121]. Here we make the assumption that $\delta\psi \sim \delta\phi$, which is correct up to a numerical pre-factor of order unity in the stationary phase approximation, for power-law de-phasing prescriptions [115]. Of course, this shortcut is only appropriate in the context of a population study, in which the intrinsic uncertainties of the environmental effect range over order of magnitudes.

B. SNR scalings for detectors with power-law sensitivity at low frequency

Adding the dephasing prescriptions of Eqs. 21 and 22 to eccentric waveform templates may allow to provide constraints on the parameters i , j , n and k , which in most cases uniquely determine the type of environmental effect. The obvious degeneracy between \mathcal{A} , i and j may perhaps be resolved if information from higher PN and eccentric harmonics is used, though this requires further investigation. Here we use their general form to calculate the expected scaling of de-phasing δSNR with binary parameters, for different detectors. This will result in a set of useful inequalities that indicate in what region of parameter space a given EE is likely to be detectable.

From Eq. 1, one can easily derive that the δSNR of a de-phased waveform roughly scales as [see e.g 34, 49, 137, among many other]:

$$\delta\text{SNR} \propto \delta\phi(f_{\text{in}}), \quad (25)$$

in the small de-phasing limit, and where we assumed that the majority of the dephasing δSNR accumulates close to the initial frequency f_{in} at which the source enters the band. From this fact alone, we can calculate expected δSNR scalings as follows. Consider a detector, the low frequency slope of which scales as f^d . Varying the source chirp mass, \mathcal{M} , changes the amplitude of the signal $A \rightarrow A'$, which in turn causes the binary to enter in the sensitivity band at a slightly different frequency

$f'_{\text{in}} = f_{\text{in}} \times (A'/A)^{1/d}$. The dephasing is then affected as:

$$\delta\phi \rightarrow \delta\phi' \propto (f'_{\text{in}})^n, \quad (26)$$

where as before the apostrophe denotes the new values after \mathcal{M} is varied. From the scalings of the de-phasing families (Eqs. 21 and 22) and the strain amplitude (Eq. 5) we find:

$$\delta\text{SNR} \propto \delta\phi(f_{\text{in}}) \propto \mathcal{M}^{(5/6) \times (n/d) + i}, \quad (27)$$

where we only considered the variation in chirp mass and used $A \propto \mathcal{M}^{5/6}$. We can repeat this series of steps for any binary parameter to find:

$$\begin{aligned} \delta\phi(f_{\text{in}}) &\propto \left(\frac{\mathcal{M}'}{\mathcal{M}}\right)^{(5/6) \times (n/d) + i} \left(\frac{\mu'}{\mu}\right)^j \\ &\times \left(\frac{D_l}{D'_l}\right)^{n/d} \left(\frac{1+z'}{1+z}\right)^{n+(5/6) \times (n/d)} \\ &\times \frac{\mathcal{F}_k(e'_{\text{in}})}{\mathcal{F}_k(e_{\text{in}})}, \end{aligned} \quad (28)$$

where the scalings originate from the variation in the frequency at which the fundamental GW mode enters the detector band. Note the complex scaling in redshift which accounts for the transformations between frequency and chirp mass in the source vs observer frame. In terms of total mass and mass ratio we have $\mathcal{M} = M(q/(1+q)^2)^{3/5}$ and $\mu = Mq/(1+q)^2$. Then the scalings read:

$$\begin{aligned} \delta\phi(f_{\text{in}}) &\propto M^{(5/6) \times (n/d) + i + j} \\ &\times \left(\frac{q}{(1+q)^2}\right)^{(3/5)i + (1/2)(n/d) + j}. \end{aligned} \quad (29)$$

We can now include the effect of the binary signal itself, and integrate over the chirp. We limit our calculations to detectors with an approximately flat sensitivity curve over several frequency decades, which approximates all detectors for sources that chirp significantly. For a detector with flat sensitivity, $S_n \propto f^{-1}$, and according to Eq. 3 and Eq. 5, $\text{SNR}_{\text{vac}}^2 \propto \int f^{-14/6+1}$. Therefore, the vacuum SNR of vacuum waveforms scales as $\propto f^{-1/6}$ [see also]. This is a very shallow power law, which shows that the total SNR depends strongly on both the initial (f_{in}) and final (f_{fin}) frequency of the observation. In terms of the δSNR we have instead:

$$\frac{d}{df} (\delta\text{SNR}(f)^2) \propto \frac{\tilde{h}(f)^2 \delta\phi(f)^2}{S_n(f)} \propto f^{-14/6+1+2n}. \quad (30)$$

Performing the integral we have:

$$\delta\text{SNR}(f) \propto f_{\text{fin}}^{n-1/6} - f_{\text{in}}^{n-1/6}. \quad (31)$$

Considering that the parameter n is typically a negative value, we see that the integral is dominated by the initial frequency and therefore $\delta\text{SNR} \propto f_{\text{in}}^{n-1/6}$. Given that

$f_{\text{in}} \propto \mathcal{M}^{5/6 \times 1/d} D_L^{1/d} (1+z)^{5/6 \times 1/d}$ and that the vacuum $\text{SNR} \propto \mathcal{M}^{5/6} D_L^{-1}$ we obtain, for a mostly white noise detector with a low frequency slope of f^{-d} , a set of δSNR scalings:

$$\delta\text{SNR} \propto D_1^{-N/d-1} (1+z)^{n+(5/6) \times (N/d)}, \quad (32)$$

$$\delta\text{SNR} \propto M^{5/6 \times (1+N/d) + i + j}, \quad (33)$$

$$\delta\text{SNR} \propto \left(\frac{q}{(1+q)^2}\right)^{3i/5 + 1/2 \times (1+N/d) + j}, \quad (34)$$

$$\delta\text{SNR} \propto \mathcal{F}_k(e_{\text{in}}), \quad (35)$$

where we defined $N = n - 1/6$. These scalings provide us with valuable information about any given EE and dephasing prescription, just by looking at their particular set of parameters i , j and k in the dephasing families of Eqs. 21 and 22. For any given detector, we know that an EE will be most significant in a certain region of binary parameter space given by the following inequalities:

$$i \lesssim -j - \frac{5}{6} \left(1 + \frac{N}{d}\right) \implies \text{lower total mass} \quad (36)$$

$$j < -\frac{3i}{5} - \frac{1}{2} \left(1 + \frac{N}{d}\right) \implies \text{smaller mass ratio} \quad (37)$$

$$k = [0, 1, 2, 3, \dots] \implies e_{\text{in}} \approx e_k^{\text{max}}, \quad (38)$$

where we used the fact that the function $q/(1+q^2)$ is monotonic in q . These inequalities are only valid in the small de-phasing limit, and eventually loose meaning for sources with low SNR in general. Nevertheless, they shed interesting light on the nature of detecting dephasing. The first inequality states that almost any detector will be more sensitive to de-phasing for lower redshift sources. Inequality 36 is only approximate, and more accurate for low mass sources which chirp significantly before merging. It states the un-intuitive result that detectors characterised by different sensitivity slopes at low frequency will be preferentially sensitive to de-phasing in sources of different mass, all else being equal. The behaviour is as follows:

$$d < -\frac{n - \frac{1}{6}}{1 + \frac{6}{5}(i+j)} \implies \text{Det. prefers low mass}, \quad (39)$$

$$d > -\frac{n - \frac{1}{6}}{1 + \frac{6}{5}(i+j)} \implies \text{Det. prefers high mass}, \quad (40)$$

where typically $d \in (-\infty, -1)$. From these equations, we see that higher masses are always preferred whenever $i+j > -5/6$. For all other cases, the steeper the detector sensitivity curve, the more strongly low masses are preferred. Finally, the third inequality states that whether small or large mass ratios are preferred depends on all

parameters d , i , j and n . The behaviour is as follows:

$$d < -\frac{n - \frac{1}{6}}{1 + \frac{6}{5}i + 2j} \implies \text{Det. pref. unequal mass,} \quad (41)$$

$$d > -\frac{n - \frac{1}{6}}{1 + \frac{6}{5}i + 2j} \implies \text{Det. pref. equal mass,} \quad (42)$$

Note that in most cases, and in particular for high SNR sources that enter detector at high amplitudes and low frequency, $d \lesssim -3$ and both low mass and unequal mass ratios are preferred due to the corresponding increase in inspiral timescale.

These inequalities open up the intriguing possibility: To define a general a-priori way to inform Bayesian priors on what regions of parameter space are likely to contain dephasing of various forms. The priors would only depend on the detector properties and the specific choice of coefficients i , j , and n for the dephased waveform model that are used in the parameter inference. While intriguing, this argument is of course only tentative and more work is required to qualify it. Nevertheless, it is indeed the case that the only source that presents evidence for the presence of acceleration in the current LVK catalogue is GW190814 [138], which showcases a relatively low total mass of $\sim 25 M_\odot$ and a mass ratio of around 10 [139].

IV. ASTROPHYSICAL DEPHASING PRESCRIPTIONS

We now turn our attention to specific models of EE, which are known to affect binaries in realistic astrophysical settings. We select or derive five different dephasing prescriptions, with the justification that their respective EE must necessarily arise as a consequence of the astrophysical formation channel of stellar mass binary BHs, in particular the dynamical channel and the AGN channel. As detailed in section II, we make the simplifying assumption that the population distributions of these channels are broadly consistent with the observed distributions in LVK. Their efficiency, i.e the ratio of the rate at which they produce GW sources, is described simply by an efficiency fraction ϵ_{DYN} and ϵ_{AGN} , respectively.

A. Dephasing due to Roemer delays

GW phase shifts due to Roemer delays arise in triple systems when the inspiralling binary's centre of mass is accelerated around a tertiary on timescales comparable to the GW driven inspiral. The phase shift is produced by means of a time dependent Doppler shift, as in Eq. 15. This means that Roemer dephasing belongs to the dephasing Family I. Identifying Roemer delays in GW signals has first been proposed in [37] and later extended

to eccentric inner binaries and eccentric outer binaries [61, 63, 117]. However, their detectability as a function of binary and GW detector properties has not been extensively studied. Here we adopt the following formula for dephasing due to Roemer delays, derived in [61]:

$$\delta\phi_{\text{R}} = \left(\frac{5}{256\pi^{13/6}}\right)^2 \frac{c^9 m_3 f_{\text{p}}^{-13/3}}{R^2 G^{7/3} \mathcal{M}^{10/3}} \times \frac{(1 + e(f_{\text{p}}))^7}{(1 - e(f_{\text{p}}))^{-1/2}}. \quad (43)$$

Note that here f_{p} is the (redshifted) GW binary's peak frequency, rather than the frequency of the fundamental GW mode. Here m_3 is the tertiary's mass and R is the distance of the tertiary to the centre of mass of the inner binary. We relate the binary's peak frequency to the fundamental GW frequency f by means of the following fit [140]:

$$f_{\text{p}} \approx f_z \left(1 + \sum_{i=1}^4 c_i e^i\right) (1 - e^2)^{-3/2}, \quad (44)$$

where $c_1 = -1.01678$, $c_2 = 5.57372$, $c_3 = -4.9271$ and $c_4 = 1.68506$. Note that here we introduced $f_z = f(1+z)$ in order to account for cosmological redshift. Evaluated at typical scales, the magnitude of Roemer dephasing for low eccentricity sources reads:

$$\delta\phi_{\text{R}}^{e=0} \approx 0.12 \times \left(\frac{m_3}{R^2} \frac{\text{AU}^2}{10 M_\odot}\right) \left(\frac{10 M_\odot}{\mathcal{M}}\right)^{10/3} \left(\frac{1 \text{ Hz}}{f_z}\right)^{13/3}, \quad (45)$$

This particular form of dephasing has a large magnitude, showing how Roemer delays may have ample prospects for detectability [61, 63], in particular when considering chaotic three-body scattering events [62]. Reading off the various power laws in the equations above, we identify the dephasing family parameters for Roemer delays: $i_{\text{R}} = -10/3$, $j_{\text{R}} = 0$, $k_{\text{R}} = 0$ and $n_{\text{R}} = -13/3$. From the inequalities in Eq. 36, we can compute that for detectors with slopes steeper than $d = -11/9$, low total mass is preferred. This is the case for all detectors here considered. Similarly, unequal mass ratios are also preferred for all detectors. Finally, we see that the defining environmental parameter for Roemer delays is $\xi_{\text{R}} = m_3/R^2$.

B. Tidal binding energy due to tertiary.

Tidal forces arise whenever a third massive body is present in the vicinity of the inspiralling binary. This is a necessary part in both the dynamical formation channel, in which binaries are driven to merger by interactions with other bodies, as well as the AGN formation channel, which necessarily entails the presence of a nearby massive BH. Tidal effects perturb the binary in several distinct

ways, which all may induce phase shifts. The most studied is the von Zeipel-Kozai-Lidov [ZKL 141–143] effect, which consists of an exchange between inner binary eccentricity and inclination and can accelerate the coalescence of compact object binaries [72, 144–151]. Instead of presenting an exhaustive list of all possible tidally induced perturbations, here we simply analyse the induced change to the binary’s binding energy, ΔE_B , as a proxy for any first order tidal EE. The latter is given by [152].

$$\Delta E_B = -\frac{1}{4} \frac{Gm_3\mu a^2}{R^3} (1 - e^2) (1 - 3\sin^2\iota \sin^2\omega), \quad (46)$$

where ι is the inclination between binary and tertiary orbital angular momentum vectors and ω is the argument of periapsis of the inner binary. As discussed in section II [see also 35, 49], any additional binding energy requires time to be radiated away via GW. This results in a modification to the GW driven inspiral timescale T_{in} with respect to a vacuum binary [49]:

$$T_{\text{in}} = T_{\text{in}}^{\text{vac}} \left(1 + 4 \frac{\Delta E_B}{E_B} \right) \quad (47)$$

Consider now the total phase of a GW signal:

$$\phi \sim \int f dt \sim f T_{\text{in}}, \quad (48)$$

where once again in the last step we assumed almost monochromatic sources. A change in inspiral timescale automatically produces a change in total phase, and thus a phase shift:

$$\delta\phi \sim 2\pi f T_{\text{in}} \times 4 \frac{\Delta E_B}{E_B}. \quad (49)$$

For concreteness, we assume that the binary is co-planar with the tertiary, such that the factor $3\sin^2\iota \sin^2\omega$ vanishes. Then, we can write down a simple prescription for the dephasing that is caused by the dissipation of tidal binding energy:

$$\frac{\delta\phi_{\text{TBE}}}{1 - e^2} = \frac{5f_z^{-11/3}}{64\pi^{11/3}} \frac{Gm_3}{R^3} \left(\frac{GM}{c^3} \right)^{-5/3} \frac{R(e)}{F(e)}, \quad (50)$$

where accounts for the redshift in frequency. For typical parameters, we have:

$$\begin{aligned} \delta\phi_{\text{TBE}}^{e=0} &\approx 0.7 \times 10^{-9} \\ &\times \left(\frac{m_3 (1 \text{ AU})^3}{R^3 10 M_\odot} \right) \left(\frac{10 M_\odot}{\mathcal{M}} \right)^{5/3} \left(\frac{1 \text{ Hz}}{f_z} \right)^{11/3}. \end{aligned} \quad (51)$$

We immediately see that dephasing to the tidal binding energy of the binary is negligible with respect to Roemer delays at relatively large distances. It does however increase rapidly with decreasing tertiary separation R . Furthermore, tidal forces may well be produced by a

large neighbouring BH with arbitrarily large mass. Finally, dephasing due to tidal effects presents an interesting angular dependence that can distinguish it from Roemer delay induced dephasing.

Due to the linear scaling with the inspiral timescale, dephasing to tidal binding energy belongs to Family II. Its dephasing family parameters are $i_{\text{TBE}} = -5/3$, $j_{\text{TBE}} = 0$, $k_{\text{TBE}} = 0$ and $n_{\text{R}} = -11/3$. The inequalities in Eq. 36, show that, low mass and unequal mass ratio sources are preferred whenever the detector sensitivity curve is steeper than $d < -11/3$. This is the case only for high SNR sources that enter the band of detector high, where sensitivity curves are generally steeper, see Figs 2 and 4. However, the opposite is true for lower SNR sources, that enter detector bands in a more shallow region of the sensitivity. Finally, we see that the defining environmental parameter for dephasing due to tidal binding energy is $\xi_{\text{R}} = m_3/R^3$.

C. Dephasing due to gas accretion and dynamical friction

The presence of gas plays a crucial role in the formation and assembly of compact object binaries in the AGN channel [*e.g.* 153–159]. With typical densities in the range of $\sim 10^{-12} - 10^{-9} \text{ g cm}^{-3}$ within 0.1pc of the SMBH, gas is known to drive the differential migration of embedded objects through the accretion disc, primarily through Type I or Type II migration torques, analogous to the ones studied in proto-stellar discs [160, 161]. In the AGN channel, BH binaries may be efficiently formed through the resulting BH-BH scatterings in the plane of the AGN disc through a process known as ”gas capture”, where the relative two-body energy of the objects is transferred to the local gas [156, 157, 162, 163]. It has been suggested that gas-capture binaries could account for a significant fraction of merging BBHs in AGN [164] and may explain more exotic detections such as the high mass ratio merger of GW190814 or high mass merger of GW190521 [165].

If the gas influence is sufficiently strong, it will have a residual effect on the inspiral of binaries even in the GW driven regime, producing potentially detectable EE. In this work, we analyse the two most obvious effects of gas on the orbital elements of an embedded binary, noting however that the hydrodynamics of embedded objects in accretion discs is highly complex, and subject of innumerable theoretical and numerical works [154, 156, 159, 166, 167]. The results here presented are therefore only to be understood as representative scalings and order of magnitude approximations of what are inevitably extremely complex physical processes. With this understanding in mind, the first qualitative effect of the presence of a surrounding gas medium is to induce an effective drag force on the binary components as a result of accretion from the medium onto the binary centre of mass [168, 169]. Here we model this with the commonly

adopted Bondi-Hoyle-Littleton (BHL) formula [170]:

$$|\vec{F}_{\text{BHL}}| = \frac{4\pi G^2 M^2 \rho}{c_s^2 + v_{\text{rel}}^2}, \quad (52)$$

where ρ is the local gas density, c_s is the local speed of sound and v_{rel} is the relative velocity of the binary's centre of mass with respect to the gas. BHL drag represents the case in which accretion is only resisted by gas pressure, and the detailed physics of the interaction of the binary with the gas are neglected. We use it here as a simple limiting case, where more detailed discussions.

In our particular case, the relative velocity term in Eq. 52 should be neglectable by only considering binaries that orbit the central SMBH on a close to circular orbit, corotating with the accretion disc gas³. To turn the drag force into a dephasing prescription, we average the power P that is exchanged with the individual binary components over an orbit:

$$P_{\text{BHL}} = \frac{1}{2\pi} \int_0^{2\pi} \vec{F}_{\text{BHL}} \cdot \vec{v}(\nu') d\nu', \quad (53)$$

where ν is the true anomaly. We can then relate the power to a drift in semi-major axis using the Newtonian relation $E = -GM\mu/(2a)$. Expressed in terms of GW frequency we have:

$$\dot{f}_{\text{BHL}} = -\frac{12f^{2/3}(GM)^{5/3}\rho}{c_s^2\mu} \times \mathcal{F}_{\text{BHL}}^{\text{sub}}(e) \quad (54)$$

where $\dot{f}_{\text{BHL}} = P_{\text{BHL}}/(dE/df)$, and E is the binary's energy. Here:

$$\mathcal{F}_{\text{BHL}}(e) = 1 + \frac{3e^2}{4} + \frac{33e^4}{64} + \frac{107e^6}{256} + \dots \quad (55)$$

is a function of eccentricity, that does not have a simple closed form [see also 171]. As expected, BHL drag belongs to the dephasing family I. Similarly to before, we can compute the expected dephasing due to BHL drag in the monochromatic approximation:

$$\begin{aligned} \delta\phi_{\text{BHL}} &= \frac{75}{16384\pi^{11/3}} \frac{c^{10}\mathcal{M}^{5/6}\rho f_z^{-14/3}}{c_s^2 G^{5/3}\mu^{7/2}} \\ &\times \frac{\mathcal{F}_{\text{BHL}}(e)R(e)^2}{F(e)^2}. \end{aligned} \quad (56)$$

For typical values gives:

$$\begin{aligned} \delta\phi_{\text{BHL}}^{e=0} &\approx 1.3 \\ &\times \left(\frac{\rho}{c_s^2} \frac{(10^4 \text{ m/s})^2}{10^{-10} \text{ g/cm}^3} \right) \left(\frac{\mathcal{M}}{10 \text{ M}_\odot} \right)^{5/6} \\ &\times \left(\frac{5 \text{ M}_\odot}{\mu} \right)^{7/2} \left(\frac{1 \text{ Hz}}{f_z} \right)^{14/3}. \end{aligned} \quad (57)$$

We can read off the BHL drag dephasing family parameters as $i_{\text{BHL}} = 5/6$, $j_{\text{BHL}} = -7/2$, $k_{\text{BHL}} = 0$ and $n_{\text{BHL}} = -14/3$. From the inequalities of Eqs. 36, we see BHL drag de-phasing will be preferred for low total masses, provided that the detector sensitivity slope is steeper than $d < -70/33$, and unequal mass ratios for a slope steeper than $d < -14/15$. The environmental parameter for dephasing due to BHL drag is $\xi_{\text{BHL}} = \rho/c_s^2$.

Taking Eq. 52 and setting instead the speed of sound to be $c_s = 0$, we recover the functional form of dynamical friction drag in the supersonic limit, i.e. a $1/v^2$ drag [172]. This represents the case of drag acting locally on the two individual binary components, which are orbiting around each other at high speed with respect to a hypothetically slow and cold ambient medium. This form of drag represents another limiting case, which is often used as a comparison to numerical investigations, even in the context of fully relativistic treatments of orbiting black holes [173]. Similarly to before, we derive the resulting dephasing prescription without thoroughly discussing the validity of Eq. 52, as it simply provides well motivated physical scaling and a typical order of magnitude estimate.

Repeating the steps above for supersonic drag, we have:

$$\dot{f}_{\text{sup}} = -\frac{12GM\rho}{\mu} \times \mathcal{F}_{\text{BHL}}^{\text{sup}}(e) \quad (58)$$

Here:

$$\mathcal{F}_{\text{sup}}(e) = 1 - \frac{e^2}{4} - \frac{7e^4}{64} - \frac{17e^6}{256} + \dots \quad (59)$$

The expected dephasing due to supersonic drag in the monochromatic approximation reads:

$$\begin{aligned} \delta\phi_{\text{sup}} &= \frac{75}{16384\pi^{13/3}} \frac{c^{10}\rho f_z^{-16/3}}{G^{7/3}\mathcal{M}^{5/6}\mu^{5/2}} \\ &\times \frac{\mathcal{F}_{\text{sup}}(e)R(e)^2}{F(e)^2}. \end{aligned} \quad (60)$$

For typical values:

$$\begin{aligned} \delta\phi_{\text{sup}}^{e=0} &\approx 4.5 \times 10^{-12} \\ &\times \left(\frac{\rho}{10^{-10} \text{ g/cm}^3} \right) \left(\frac{10 \text{ M}_\odot}{\mathcal{M}} \right)^{5/6} \\ &\times \left(\frac{5 \text{ M}_\odot}{\mu} \right)^{5/2} \left(\frac{1 \text{ Hz}}{f_z} \right)^{16/3}. \end{aligned} \quad (61)$$

We can read off the supersonic drag dephasing family parameters as $i_{\text{BHL}} = -5/6$, $j_{\text{BHL}} = -5/2$, $k_{\text{BHL}} = 0$ and $n_{\text{BHL}} = -16/3$. From the inequalities of Eqs. 36, we see that BHL drag de-phasing will also be preferred for low total masses and unequal mass ratios. The environmental parameter for dephasing due to BHL drag is $\xi_{\text{BHL}} = \rho$.

³ In the general case a binary on an eccentric orbit may transition between the sub-sonic and the super-sonic regimes, producing complex accretion patterns and drag forces

D. Dephasing due to circumbinary disc torques

Our analysis of BHL and supersonic drag neglects various aspects of the interaction between the binary and the accretion flow. Binaries surrounded by cold gas are typically described by a viscous circumbinary disc, rather than a radial Bondi flow. Details of the accretion flow are complex and the subject of numerous theoretical and numerical investigations (see e.g. [174] for a review), but a typical feature is that a near equal-mass binary carves an evacuated central cavity of characteristics size $r_{\text{in}} \approx 2a$. A simple analysis (and converse to the pure accretion drag) is that for a system where the tidal barrier of the rotating binary potential identically balances the viscous angular momentum flux at this cavity edge.⁴ If the accretion rate is mediated by viscosity alone, it is given by [175, 176]:

$$\dot{M} \sim 3\pi r^2 \Sigma \tau_{\text{visc}}^{-1} \quad (62)$$

where τ_{visc} is the viscous timescale, Σ is the gas surface density and r is a radial coordinate. For a classical α -disk [175], this causes the binary orbit to decay at the associated viscous rate:

$$\frac{a_{\text{CBD}}}{a} = -48\pi\alpha \frac{c_s^2 \Sigma}{\mu \sqrt{1-e^2}} f_z^{-1} \quad (63)$$

where $\alpha \lesssim 1$ characterizes the magnitude of disk stresses. Similar to above we can compute the dephasing due to viscous torques in the monochromatic approximation:

$$\delta\phi_\alpha = -\frac{225}{8192\pi^{10/3}} \frac{\alpha c^{10} c_s^2 \Sigma f_z^{-16/3}}{G^{10/3} \mathcal{M}^{10/3} \mu} \times \frac{R(e)^2}{\sqrt{1-e^2} F(e)^2}. \quad (64)$$

Note that here we have assumed that the cavity edge and the binary remain coupled until the end of the inspiral. Whether or not such binary-disk decoupling occurs in reality remains an active line of study [177–180], and will not be discussed in detail.

Eq. 64 represents a model for dephasing for a binary embedded in an isolated, viscous circumbinary disc. However, for binaries embedded in AGN disc, the circumbinary disc will necessarily be embedded in a larger system that may supply gas and angular momentum at higher rates. As an example, mechanisms such as shear or large scale magnetic fields may act to replenish the cavity faster than viscosity alone. In the limiting case, the driving mechanism to drive the angular momentum flux in the circumbinary disc can be characterised by a fast, dynamical timescale. In our setup, the dynamical

timescale is the binary’s orbital timescale τ_{orb} around the central massive black hole. Note that this is also equal to the orbital timescale at the binary’s Hill sphere, at which the circumbinary disc is coupled to the larger scale AGN disc. With respect to viscosity alone, the angular momentum flux would then be increased by a factor:

$$\begin{aligned} \frac{\tau_{\text{visc}}}{\tau_{\text{orb}}} &= \frac{\sqrt{GM_{\text{MBH}}}}{2\pi\alpha c_s H R^{1/2}} \\ &\approx 6.8 \times 10^4 \frac{0.1}{\alpha} \left(\frac{10^4 \text{ m/s}}{c_s} \right)^2 \left(\frac{M_{\text{MBH}}}{10^8 M_\odot} \right) \left(\frac{0.1 \text{ pc}}{r} \right)^2, \end{aligned} \quad (65)$$

where $H \sim c_s/\Omega_K$ is the scale height of the disc. Therefore, at typical separations for binaries in the AGN channel, it is exceedingly likely that viscous torques alone are a gross underestimation for the evolution of the binary elements. To model this effect, we introduce a simple fudge factor f_{CBD} to Eq. 64, while preserving the scaling appropriate for the evolution of binaries in circumbinary discs:

$$\begin{aligned} \delta\phi_{\text{visc}} &= -\frac{225 f_{\text{CBD}}}{8192\pi^{10/3}} \frac{\alpha c^{10} c_s^2 \Sigma f_z^{-16/3}}{G^{10/3} \mathcal{M}^{10/3} \mu} \\ &\times \frac{(1+e^2) R(e)^2}{F(e)^2}. \end{aligned} \quad (66)$$

Once again, f_{CBD} can potentially be of the order 10^4 or more depending on the AGN disc model and the detailed hydrodynamics of the embedded binary. For typical values, the dephasing then reads:

$$\begin{aligned} \delta\phi_{\text{visc}}^{e=0} &\approx 1.3 \times 10^{-4} \\ &\times \frac{\alpha f_{\text{CBD}}}{10^3} \left(\frac{\Sigma}{10^6 \text{ g/cm}^2} \right) \left(\frac{c_s^2}{10^4 \text{ m/s}} \right) \left(\frac{10 M_\odot}{\mathcal{M}} \right)^{10/3} \\ &\times \left(\frac{5 M_\odot}{\mu} \right) \left(\frac{1 \text{ Hz}}{f_z} \right)^{16/3}. \end{aligned} \quad (67)$$

Summarising, we see that dephasing due to circumbinary disc torques belongs to family I, and has the parameters $i_\alpha = -16/3$, $j_\alpha = -1$, $k_\alpha = 0$ and $n_\alpha = -16/3$. It will be preferred for lower mass binaries for detectors with a slope steeper than $d < -80/63$, and unequal mass ratios for detectors with $d < -16/15$. The environmental parameter for dephasing due to circumbinary torques is $\xi_\alpha = \alpha\beta\Sigma c_s^2$.

E. Summary

Table I summarises the family parameters of the five astrophysical dephasing prescriptions we collected or derived. Fig. 4 shows their evolutionary paths for an exemplary eccentric binary, as a function of the fundamental GW frequency. Note how the different combination of frequency scaling and eccentricity extensions give rise to

⁴ In this picture, no material penetrates the cavity and the binary accretion rate is zero.

EE	Family	ξ	i	j	n
Roemer	I	m_3/R^2	-10/3	0	-13/3
Tidal BE	II	m_3/R^3	-5/3	0	-11/3
BHL drag	I	ρ/c_s^2	5/6	-7/2	-14/3
Sup drag	I	ρ	-5/6	-5/2	-16/3
CBD torques	I	$\alpha f_{\text{CBD}} \Sigma c_s^2$	-10/3	-1	-16/3

TABLE I. Dephasing family parameters of the five dephasing prescriptions treated in this paper. The parameters uniquely identify the EE, and also indicate the preferred parameter space in which to search for the corresponding de-phasing.

unique and potentially distinguishable behaviour. Furthermore, we show a parameter space plot comparing detector slopes and the dephasing family parameters for our choice of prescriptions. Typical detectors will have sensitivity curves with relatively steep slopes at lower frequencies, meaning that dephasing is typically more easily detectable for lower mass sources. In some cases however, e.g. the shallow part of ET’s sensitivity curve between ~ 1 Hz and ~ 8 Hz, an increase in mass can disproportionately increase the total amount of accumulated dephasing by lowering the initial frequency of the observation. These results indicate how the dephasing prescriptions of several crucial EE have unique high eccentricity extensions as well as interactions with different detectors.

V. FRACTION OF SOURCES WITH SIGNIFICANT DEPHASING

We now detail our strategy to estimate the fraction of sources that will showcase EE for different detectors. We can evaluate Eq. 1 for an appropriate grid of parameters, after selecting a given dephasing prescription and GW detector. To expedite calculations, we base the results on a reference value of the appropriate environmental parameter ξ_{ref} . The parameter ξ_{ref} is chosen such that the evaluated δSNR is small, and respectively the dephasing caused by the EE is $\ll \pi$. In this way, we can rescale the δSNR results for any choice of ξ by simply multiplying by the factor ξ/ξ_{ref} . The result of this procedure is a series of 20 re-scalable, four-dimensional cubes containing the δSNR contours for the dephasing prescriptions detailed in section IV.

In Appendix A (and B for LISA), we show several 2-d slices of these “ δSNR cubes”, focusing on the detector ET. We see how the δSNR of different dephasing prescriptions scale as a function of the binary parameters, producing complex contours. The shapes of these contours are already quite rich and informative. They represent the numerical counterpart to the discussion of the interaction between dephasing family parameters and detector sensitivity slopes in section III. Here we refrain from a thorough discussion, and focus instead on integrating the δSNR cubes over the population parameter distributions.

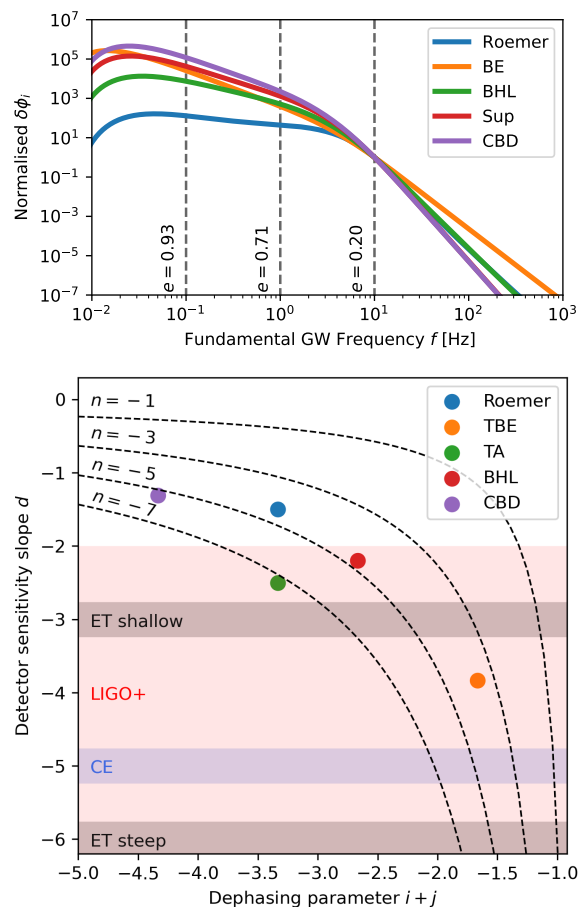


FIG. 4. Top panel: evolutionary paths for the five dephasing prescriptions analysed in this work, for a binary with an eccentricity of 0.2 at 10 Hz. The magnitude is normalised. Bottom panel: parameter space plot comparing detector slopes and the dephasing family parameters (see Eqs. 21 and 22). Plotted are the lines (dashed black) under which a given detector will be more sensitive to dephasing for lower mass sources, given a dephasing prescription with fixed n and $i + j$. The five specific dephasing prescriptions analysed in this work are shown as coloured dots. The shaded areas denote the approximate ranges for the slopes of three ground based detectors ET, CE and LIGO (A+ and A#) (see also Fig. 2). LIGO sensitivity curves span through a large range of slopes due to the characteristic curved shape (see Fig. 2). The plot shows how, depending on the specific detector-dephasing prescription combination, it will be more promising to look for EE in higher vs lower mass sources. In the typical case, lower mass sources are more promising in terms of dephasing for steep detector sensitivity curves.

Our goal is to estimate the detection fraction of sources with significant dephasing as a function of the environmental parameters ξ . To this purpose we employ a Monte Carlo integration scheme. First, we wish to identify the phase space volume V_{det} of all sources that are detectable by a given detector. We sample binary mass, mass ratio, redshift and eccentricity randomly from the following

ranges:

$$M_i \in (5 M_\odot, 200 M_\odot) \quad (68)$$

$$q_i \in (0, 1) \quad (69)$$

$$z_i \in (0, 5) \quad (70)$$

$$e_i^{10\text{Hz}} \in (0, 0.2). \quad (71)$$

Then, we evaluate the SNR of a vacuum waveform with the sampled parameters. Note here that ET and CE are sensitive to sources with masses larger than the current upper limit of $200 M_\odot$. We introduce this cutoff because the distribution of such sources is entirely unconstrained, and to expedite the convergence of the integration. The phase space volume of detectable sources, for which we use the standard criterion of $\text{SNR} > 8$, is given by the following weighted sum:

$$V_{\text{det}} \approx \sum_i^N \Theta(\text{SNR}_i - 8) \times w(M_i, q_i, z_i, e_i^{10\text{Hz}}), \quad (72)$$

where Θ is a Heaviside function the w are weights that encode the probability of finding a source with a given set of parameters. In our case, we have $w \equiv \mathcal{P}$, as detailed in section II C. We proceed similarly to compute the phase-space volume V_{EE} for which an EE dephasing prescription with a given parameter ξ is significant (and perhaps detectable assuming that appropriate waveforms exist), i.e. it reaches a $\delta\text{SNR}=3$:

$$V_{\text{EE}} \approx \sum_i^N \Theta(\delta\text{SNR}_i - 3) \times w(M_i, q_i, z_i, e_i^{10\text{Hz}}). \quad (73)$$

The fraction of sources that will showcase a significant dephasing is calculated simply by dividing the two volumes, while multiplying by the appropriate formation channel's efficiency parameter ϵ .

$$\text{Detection fraction} = \epsilon \frac{V_{\text{EE}}}{V_{\text{det}}}. \quad (74)$$

We test the convergence of the integration by evaluating the volumes for a few random realisations at a given resolution and checking if the results remain unaffected, which is achieved for $N \sim 10^8$. For simplicity, we now omit to specify the efficiencies of the dynamical and AGN channel, i.e. our results are quoted for $\epsilon_{\text{dyn}} \sim 1$ and $\epsilon_{\text{AGN}} \sim 1$.

A. Detection fractions and required environmental properties

We repeat the procedure detailed above for each combination of detector and dephasing prescription. The results of this are shown in Fig. V A, Fig. V A 3 as well as Table II and most conclusions can be drawn directly from the plots. We will now briefly discuss the results and highlight some additional points for each individual

dephasing prescription, while overall conclusion is presented in section VI. Here we note once again that the results presented in this section are informed by the following aspects:

- The scalings and functional form of the various dephasing prescriptions (see Eqss 21 and 22.)
- The interaction of said dephasing prescriptions with the detector sensitivity curves (see Fig. 4).
- The observed distribution of stellar mass BH binaries and their detectability as a function of redshift, mass and mass ratio (see section II C).

1. Roemer Delays

The typical value of the Roemer delay environmental parameter $\xi_{\text{R}} = m_3/R^2$ depends on the third body in the vicinity of the binary. Here we focus on mergers resulting from 3-body scatterings in clusters, which are known to be able to produce a significant rate of mergers as well as mergers with residual eccentricity. As a rough estimate, we expect m_3 to range from a few to a few hundreds of M_\odot , while R is related to the velocity dispersion of the cluster in which the 3-body scattering take place. As discussed in [62], we expect $R \sim 1 \text{ AU}$, $R \sim 0.1 \text{ AU}$ and $R \sim 0.01 \text{ AU}$ for typical globular clusters, dense stellar clusters and nuclear star clusters, respectively. As seen in Fig. V A and Table II a significant fraction of GW signals (1% to 10%) will showcase significant dephasing due to Roemer delays for a parameter $\xi_{\text{R}} \sim 100 M_\odot/\text{AU}^2$ to $\sim 1000 M_\odot/\text{AU}^2$, for next generation space based detectors. This is not only possible, but *expected* for binaries that merge as a result of scatterings in stellar clusters. We note here, that dephasing due to Roemer delays should be significant in *all* binary mergers that occur as a result of scattering in nuclear clusters, which may account for merger rates of up to $\mathcal{O}(10) \text{ Gpc}^{-1} \text{ yr}^{-1}$ [181, 182]. For mergers due to binary-single scatterings in an AGN disc, the dephasing could be significantly increased as the surrounding gas can harden the triple system, substantially reducing R in the leadup to merger [183].

The magnitude of the Roemer dephasing may be even larger than expected from our model, in which we consider the binary orbit around the third object to be circular. Curvature effects from *eccentric* orbits around the third object, which are a common occurrence in clusters, can give rise to increased Roemer dephasing several orders of magnitude higher than the circular case [63]. Additionally statistical outliers that result from strong chaotic scatterings, as discussed in [62]. We also note that, without considering the effect of eccentric waveforms, differences in the underlying binary eccentricity distribution do not influence our conclusions.

Roemer delays also play a significant role in the AGN channel, in which binaries may be orbiting close to the

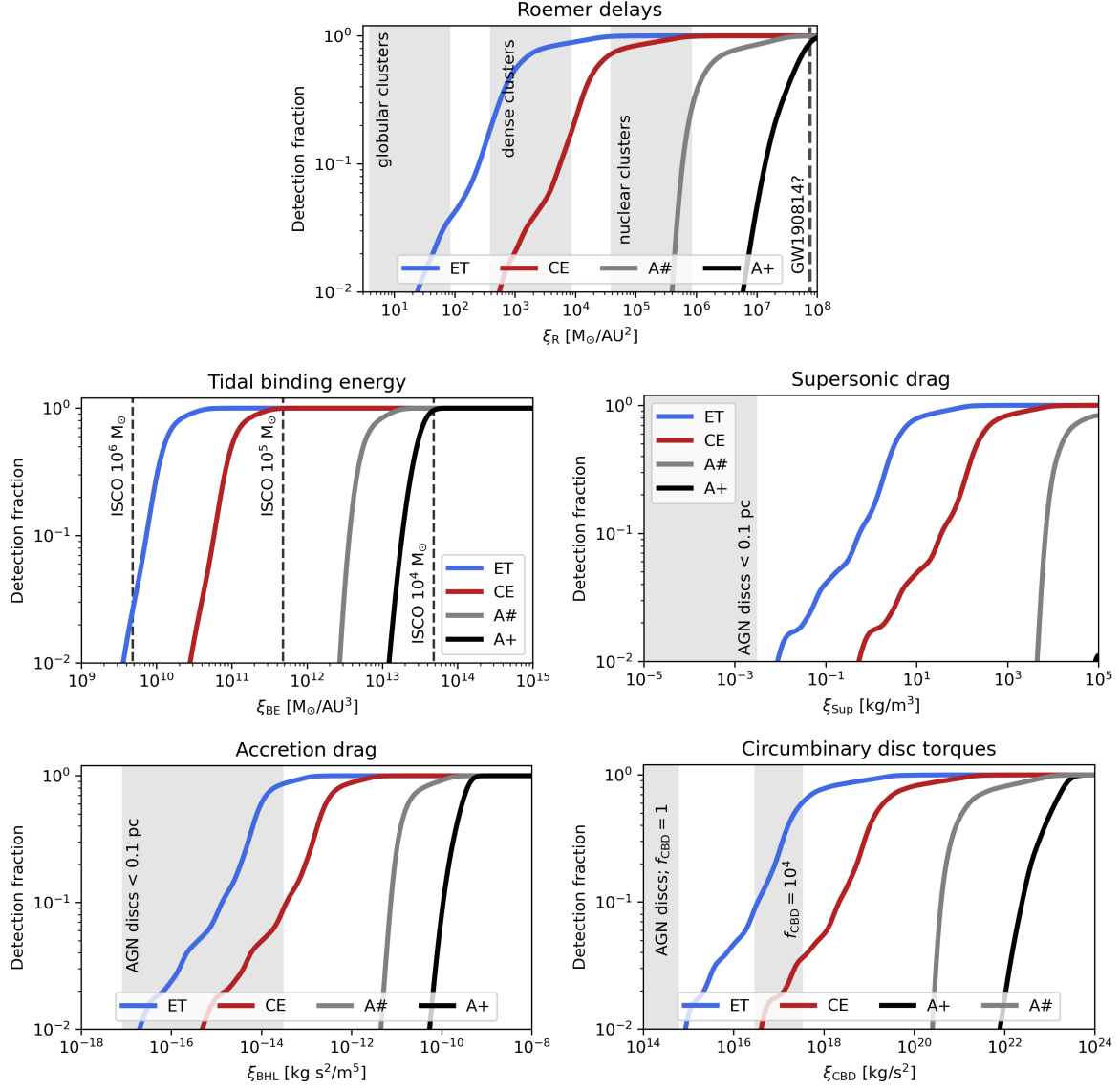


FIG. 5. The expected detection fractions of sources for LIGO A+ (black), CE (red) and ET (blue), as a function of the appropriate environmental parameter ξ . The grey shaded areas and vertical grey lines denote reference ranges and values that could be expected in typical astrophysical systems (see text). The graphs assume the observed LVK population distributions and a formation channel efficiency of $\epsilon = 1$. We see that third generation ground based such as ET and CE are will be expected to showcase dephasing in a substantial fraction of sources.

central BH. rescaled to our typical units, we find the value for the parameter ξ_R for a binary orbiting a SMBH at a radius R :

$$\xi_R \approx 2.6 \times 10^3 \times \left(\frac{10^3 r_S}{R} \right)^2 \quad (75)$$

$$\times \left(\frac{M_{\text{SMBH}}}{10^6 M_\odot} \right) [\text{M}_\odot/\text{AU}^2]$$

We see that Roemer delays should lead to a significant fraction of signals with detectable phase-shifts even for typical distances of thousands of Schwarzschild radii.

The emerging picture is that Roemer delays represent

the most likely candidate for the detection of an EE in stellar mass BH binaries, and they are expected to be present in a significant fraction of the detected signals for third generation GW detectors for a wide range of the parameter ξ_R . In fact, for the large but physically plausible values of $\xi_R > 10^6 \text{ M}_\odot/\text{AU}^2$ expected for scatterings in nuclear clusters or in the AGN channel at hundreds of Schwarzschild radii, we would even expect a few percent of future LVK sources to showcase detectable dephasing signatures, in particular for light binaries with unequal mass ratios. It is intriguing to note that currently there exists a single candidate signal that showcases evidence of dephasing with a power law of $f^{-13/3}$, originating from

Det. fraction (Roem.)	A+; ξ_R [M_\odot/AU^2]	A#; ξ_R [M_\odot/AU^2]	CE; ξ_R [M_\odot/AU^2]	ET; ξ_R [M_\odot/AU^2]
0.1%	3.2×10^6	2.2×10^6	1.1×10^2	7.9×10^0
1%	6.4×10^6	4.9×10^6	5.8×10^2	2.2×10^1
10%	1.4×10^7	6.2×10^6	5.4×10^3	2.7×10^2
Det. fraction (TBE)	A+; ξ_{BE} [M_\odot/AU^3]	A#; ξ_{BE} [M_\odot/AU^3]	CE; ξ_{BE} [M_\odot/AU^3]	ET; ξ_{BE} [M_\odot/AU^3]
0.1%	1.1×10^{13}	3.3×10^{12}	1.6×10^{10}	2.4×10^9
1%	1.4×10^{13}	3.8×10^{12}	2.0×10^{10}	3.9×10^9
10%	2.1×10^{13}	4.2×10^{12}	6.5×10^{10}	8.1×10^9
Det. fraction (BHL)	A+; ξ_{BHL} [$\text{kg s}^2/\text{m}^5$]	A#; ξ_{BHL} [$\text{kg s}^2/\text{m}^5$]	CE; ξ_{BHL} [$\text{kg s}^2/\text{m}^5$]	ET; ξ_{BHL} [$\text{kg s}^2/\text{m}^5$]
0.1%	3.4×10^{-11}	2.9×10^{-12}	2.2×10^{-17}	4.6×10^{-18}
1%	6.0×10^{-11}	4.9×10^{-12}	5.6×10^{-16}	2.1×10^{-17}
10%	1.1×10^{-10}	8.2×10^{-12}	1.2×10^{-13}	1.2×10^{-15}
Det. fraction (Sup)	A+; ξ_{Sup} [kg/m^3]	A#; ξ_{Sup} [kg/m^3]	CE; ξ_{Sup} [kg/m^3]	ET; ξ_{Sup} [kg/m^3]
0.1%	4.1×10^4	3.4×10^3	4.0×10^{-2}	1.6×10^{-3}
1%	8.5×10^4	5.4×10^3	6.1×10^{-1}	9.3×10^{-3}
10%	1.0×10^5	7.4×10^3	3.6×10^1	5.6×10^{-1}
Det. fraction (CBD)	A+; ξ_{CBD} [kg/s^2]	A#; ξ_{CBD} [kg/s^2]	CE; ξ_{CBD} [kg/s^2]	ET; ξ_{CBD} [kg/s^2]
0.1%	3.4×10^{21}	2.1×10^{20}	2.4×10^{15}	2.9×10^{14}
1%	8.4×10^{21}	3.1×10^{20}	4.2×10^{16}	8.7×10^{14}
10%	2.6×10^{22}	4.0×10^{20}	2.0×10^{18}	3.2×10^{15}

TABLE II. Required magnitude of the various environmental parameters ξ_i required for various detectors to expect significant dephasing in 0.1%, 1% and 10% of detected signals. The results assume the observed LVK population distributions and a formation channel efficiency of $\epsilon = 1$.

a binary with exactly the expected properties [138]. The signal in question is GW190814, with a potential acceleration of $0.0015 \pm 0.007 c/s$, corresponding to a parameter $\xi_R = 7.6 \times 10^7 M_\odot/\text{AU}^2$. We note here that an acceleration of this magnitude would be detectable for almost 100 % of LVK sources with A+ sensitivity, and the most likely case is that this is in fact an outlier, or simply a wrong interpretation of a feature in the data. In any case, our results provide a simple way to assess whether the majority of mergers occur in environments characterised by accelerations similar to the ones experienced (allegedly) by GW190814.

2. Tidal effects

As a reference value for the environmental parameters ξ_{TBE} , we consider a binary orbiting at the innermost stable circular orbit of a supermassive black hole, which yields the following tidal parameter:

$$\begin{aligned} \xi_{\text{TBE}} &\rightarrow \frac{m_3 c^6}{27 \times 8G^3 m_3^3} \\ &\approx 4.8 \times 10^9 \left(\frac{10^6 M_\odot}{m_3} \right)^2 \frac{M_\odot}{\text{AU}^3}. \end{aligned} \quad (76)$$

Placing the binary further away would then reduce the environmental parameter with a cubic scaling. Comparing with the results displayed in Fig. V A, we see that the only scenario in which we may expect a significant frac-

tion of sources to showcase dephasing is for binaries orbiting in the close vicinity of low mass SMBHs or around intermediate mass black holes. Such systems can be realised in the AGN formation channel, due to the presence of migration traps [184], and would represent interesting laboratories to study relativistic dynamics [98, 185]. Nevertheless, our analysis suggests that dephasing due to Roemer delays is almost certainly dominant with respect to tidal effects, because of the more forgiving scaling of m_3/R^2 rather than m_3/R^3 .

3. Hydrodynamical effects

The density and speed of sound expected in accretion discs vary significantly depending on the central object mass, the specific disc model and the radius under consideration. In our analysis, we considered three prescriptions that scale differently with gas properties, as detailed in Table I. Here we base our analysis of hydrodynamical effects in AGN discs on the commonly used Sirko & Goodman α -disc model [186, 187], as implemented in the publicly available `pAGN` package. We assume for our disc models an Eddington ratio of $l_E = 0.5$, hydrogen fraction $X = 0.7$, alpha viscosity of $\alpha = 0.1$ and a radiative efficiency of $\epsilon_{\text{rad}} = 0.1$.

Fig. V A 3 displays the values of the environmental parameters ξ_{Sup} , ξ_{BHL} and ξ_{CBD} evaluated for such a disc model. Additionally, we highlight the contours that correspond to a certain detection fraction for detectors. We

summarise the results qualitatively as follows:

- For BHL drag, we find that for next generation detectors such as ET and CE, values of the environmental parameters that correspond to significant detection fraction are reached in the inner regions of the disc.
- For supersonic drag, dephasing is too small to be present in a significant fraction of sources for any of the considered detectors.
- For CBD torques, a fudge factor is required for any significant amount of sources to showcase dephasing signatures. For a constant fudge factor, wide regions of AGN discs around low mass SMBHs will produce large detection fractions. For a fudge factor proportional to the ratio of viscous to dynamical time, CBD torques are so strong that significant detection fractions are also expected with A+ sensitivity, in the inner regions of AGN around low mass SMBH.

Overall, the conclusions regarding the significance of dephasing due to hydrodynamical effects depend on the prescription that is used. Taking BHL drag as a baseline, we conclude that significant detection fractions are expected in the AGN channel for third generation detectors, not for LVK upgrades.

VI. SUMMARY AND CONCLUSION

Our work can be summarised as follows:

- We have constructed two general families of dephasing prescriptions and derived a set of inequalities that detail what regions of parameter space are more likely to showcase dephasing with different scalings. The latter may be used to inform priors in an a-priori way in parameter inference studies.
- We have collected and analysed five dephasing prescriptions that represent smoking gun physical mechanisms at play in the dynamical and AGN formation channel for stellar mass BH binary systems.
- We have computed the expected fraction of sources that will showcase significant dephasing for four upcoming ground based detector sensitivities, as a function of environmental properties. The results are visualised in Fig. V A and V A 3, as well as Table II. These results can be used as a reference to prioritise the efforts in GW modeling work, as well as inform future studies that aim to model binary environments and their coupling to binaries.

We have found that Roemer delays and hydrodynamical effects in particular can induce strong dephasing for third body properties and gas properties that are considered typical for the dynamical and the AGN formation channels, respectively. Summarising:

- For Roemer delays, accelerations that are entirely consistent with the typical environments of binaries will cause significant dephasing in $\sim 1\%$ to $\sim 100\%$ of binaries in the dynamical or AGN channel for ET and CE. At a minimum, hundreds of signals are expected showcase such signatures (see Fig V A and Table II). Roemer delay may also be relevant for a significant amount of sources with A# sensitivity, depending on the dominance of the nuclear cluster sub-channel or the AGN channel.
- For third generation detectors such as ET and CE one can expect to find significant fractions of signals with gas induced dephasing, assuming BHL drag and provided that binaries in the AGN channel merge in the inner regions of the disc (see Fig. V A 3 in combination with Table II). However, more work is required to properly model the details of accretion flows for binaries embedded in AGN, as commonly used prescriptions yield wildly varying results.

The third generation of ground based GW detectors is expected to become operational within the next decade. We believe that our work strongly indicates that EEs are not only a possibility, but are almost certainly going to be present in a significant fraction of the thousands of expected signals. To take advantage of this fact, it will be necessary to fully develop GW templates that contain EE prescriptions, and are able to extract and distinguish between EE in real GW signals. In particular, we recommend focusing on Roemer delays and its eccentricity extensions, as well as dephasing prescriptions for gas accretion and CBD torques.

Another aspect that is often neglected in discussions of binary environments is the coupling between EE and eccentricity, which is considered a smoking gun for the dynamical formation channel and perhaps for the AGN channel [159]. Our preliminary analysis of the two dephasing families in section III further solidifies the claim that eccentric dephasing prescriptions carry additional information that can be used to identify and distinguish unique properties of EE [see e.g. 70, for the similar considerations in the case of extreme mass ratio systems]. We will explore this aspect in detail in paper II. Overall, we find that the emerging picture is that the joint study of eccentricity and environmental dephasing in individual systems is likely to become a reality in the next decade. The prospects to complement current population based inferences with the detection of smoking gun signatures in individual signals are extremely rich, and will add a new tool in the rapidly growing field of gravitational wave astronomy.

ACKNOWLEDGMENTS

L.Z., J.T., P.S., J.S and K.H. acknowledge support from ERC Starting Grant No. 121817–BlackHoleMergs

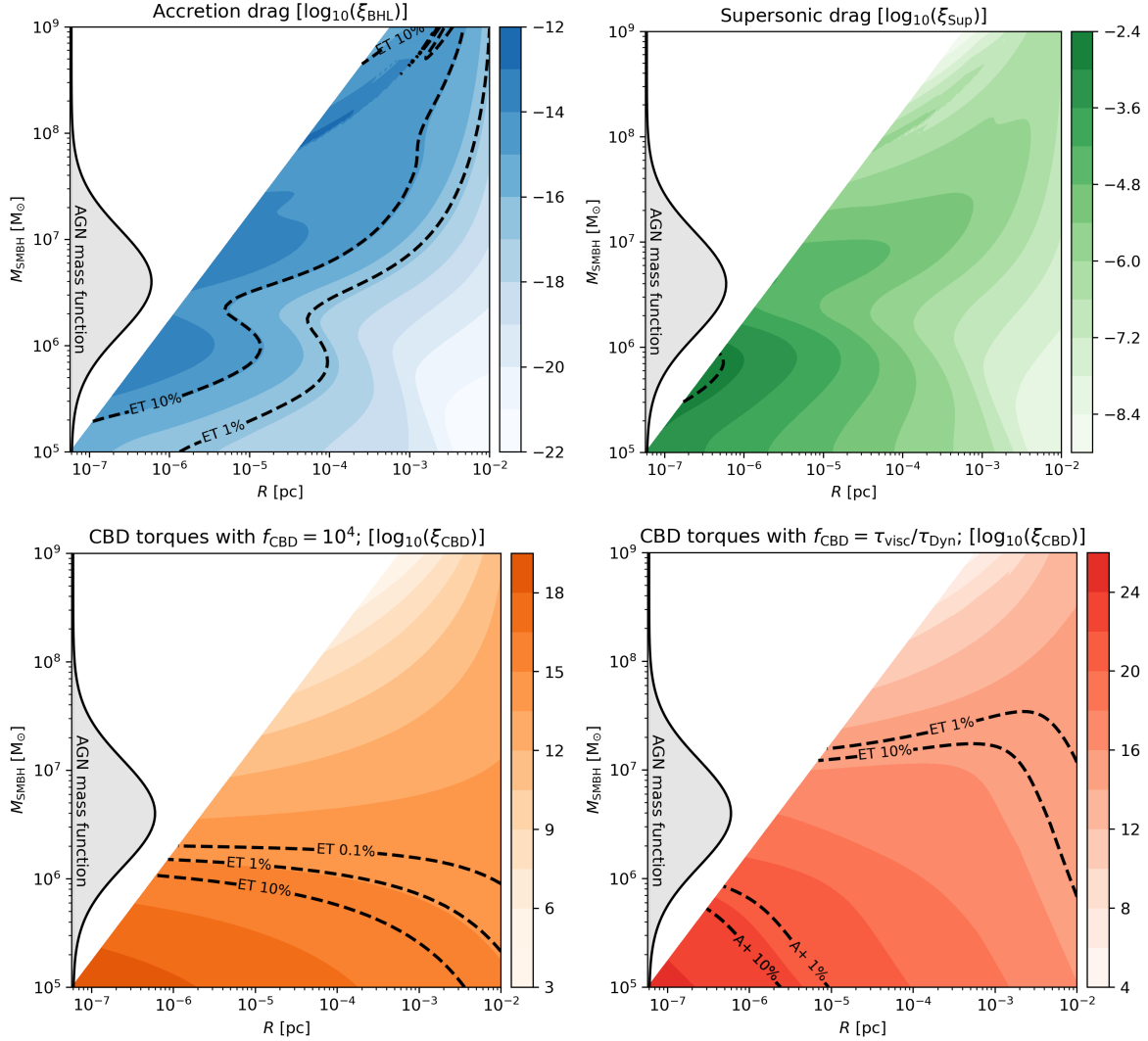


FIG. 6. Contour plots of the values of the environmental parameters $\xi_{\text{Sup}}, \xi_{\text{BHL}}$ and ξ_{CBD} (in \log_{10} , where the units are as in Table I) for a Sirko & Goodman AGN alpha disc model with $l_E = 0.5$, $X = 0.7$, $\alpha = 0.1$ and $\varepsilon_{\text{rad}} = 0.1$. We highlight contours depicting the detectability fractions of certain detectors. The plot can be understood as follows: if all BH-BH mergers occurred within the regions of the AGNs discs that corresponds to a percentage contour, then we would expect at least that percentage of sources to showcase dephasing (due to the given hydro effect for the given detector). In the case of ET and CE, 1% of sources still corresponds to hundreds of signals with significant dephasing. To suggest the most likely case we also plot the AGN mass function as fitted by [188], in gray.

led by J.S. L.Z. and J.S. are also supported by the Villum Fonden grant No. 29466. A.A.T. acknowledges support from the Horizon Europe research and innovation programs under the Marie Skłodowska-Curie grant agreement no. 101103134.

Appendix A: Phase space slices for the Einstein telescope

Fig. A shows the two dimensional slices of δSNR parameter space referenced in section V.

Appendix B: A note on space based detectors

It is interesting to repeat part of the procedures detailed in the main text for stellar mass BHs that will potentially show up in the milli-Hz band as pre-LVK sources. Here we take the LISA [60] sensitivity curve as a baseline, and integrate the SNR and δSNR of dephased GW going backwards in frequency, from the moment they exit the band to four years prior. The presence of eccentricity for such sources is much more significant as in the ground based case, as an eccentric binary can chirp over a much wider range of frequencies over the limited observation time of a space-borne GW detector (with re-

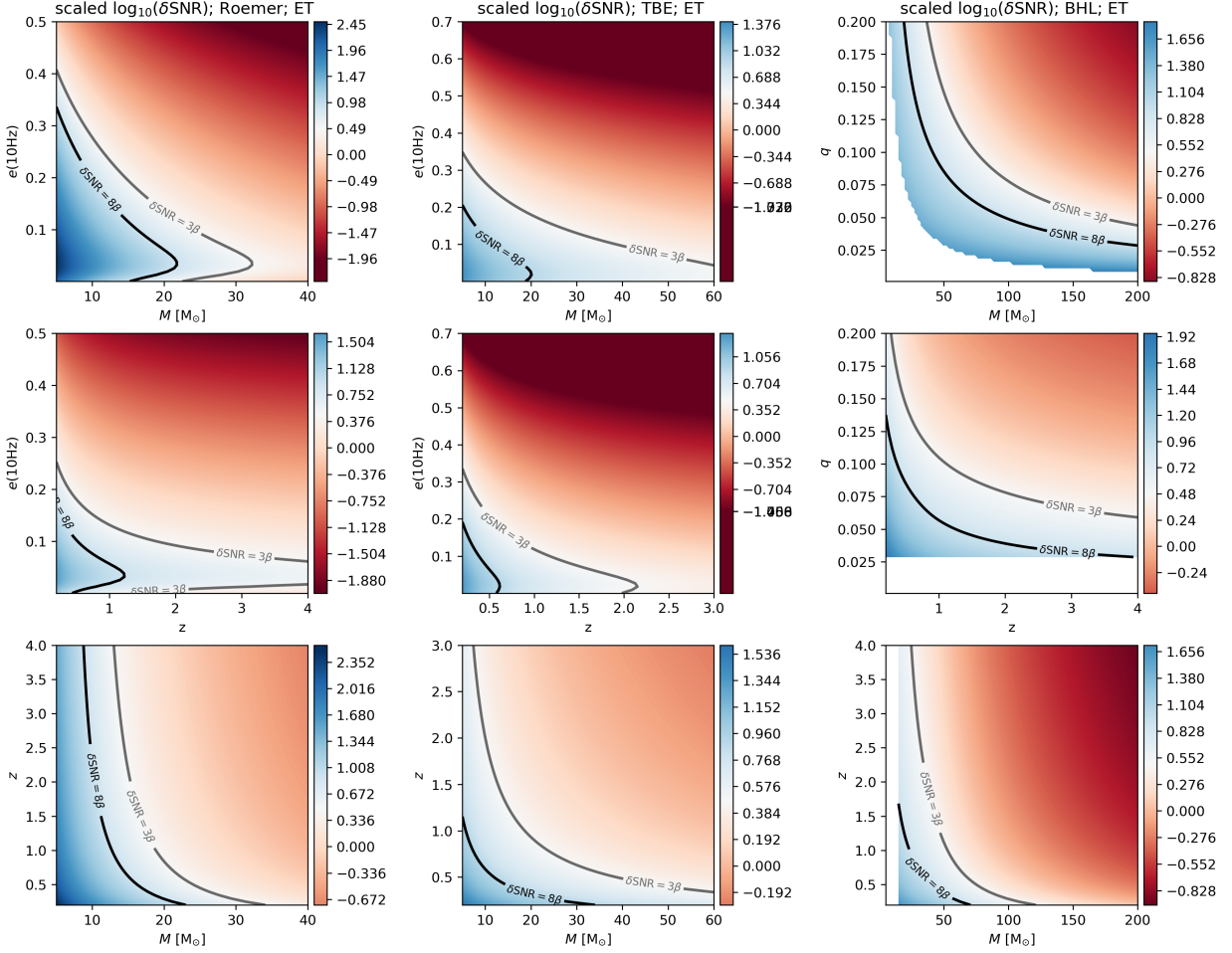


FIG. 7. Two dimensional slices of the δSNR cubes for various dephasing prescriptions with a fixed value of the parameter ξ (for ET). Note how the contours vary purely as a function of binary parameters. Blue regions of phase space are more likely to present detectable EE, all else being equal.

spect to the signal life-time). We do not discuss this in detail, as here it absolutely crucial to perform the estimates with fully eccentric waveforms. We note however the rich and interesting shapes of the slices of the δSNR results, in Fig. B. With the caveat of the rate and signal

identification challenges of such sources, looking for EE in eccentric pre-LVK binaries in LISA is potentially extraordinarily promising [see also 44], and deserves more investigation.

-
- [1] K. Belczynski, V. Kalogera, and T. Bulik, A Comprehensive Study of Binary Compact Objects as Gravitational Wave Sources: Evolutionary Channels, Rates, and Physical Properties, *Astrophys. J.* **572**, 407 (2002), [arXiv:astro-ph/0111452 \[astro-ph\]](#).
 - [2] R. M. O’Leary, R. O’Shaughnessy, and F. A. Rasio, Dynamical interactions and the black-hole merger rate of the Universe, *Phys. Rev. D* **76**, 061504 (2007), [arXiv:astro-ph/0701887 \[astro-ph\]](#).
 - [3] A. Sadowski, K. Belczynski, T. Bulik, N. Ivanova, F. A. Rasio, and R. O’Shaughnessy, The Total Merger Rate of Compact Object Binaries in the Local Universe, *Astrophys. J.* **676**, 1162 (2008), [arXiv:0710.0878 \[astro-ph\]](#).
 - [4] F. Antonini and F. A. Rasio, Merging Black Hole Binaries in Galactic Nuclei: Implications for Advanced-LIGO Detections, *Astrophys. J.* **831**, 187 (2016), [arXiv:1606.04889 \[astro-ph.HE\]](#).
 - [5] S. Vitale, R. Lynch, R. Sturani, and P. Graff, Use of gravitational waves to probe the formation channels of compact binaries, *Classical and Quantum Gravity* **34**, 03LT01 (2017), [arXiv:1503.04307 \[gr-qc\]](#).
 - [6] B. J. Kavanagh, D. A. Nichols, G. Bertone, and D. Gaggero, Detecting dark matter around black holes with gravitational waves: Effects of dark-matter dynamics on the gravitational waveform, *Phys. Rev. D* **102**, 083006 (2020), [arXiv:2002.12811 \[gr-qc\]](#).

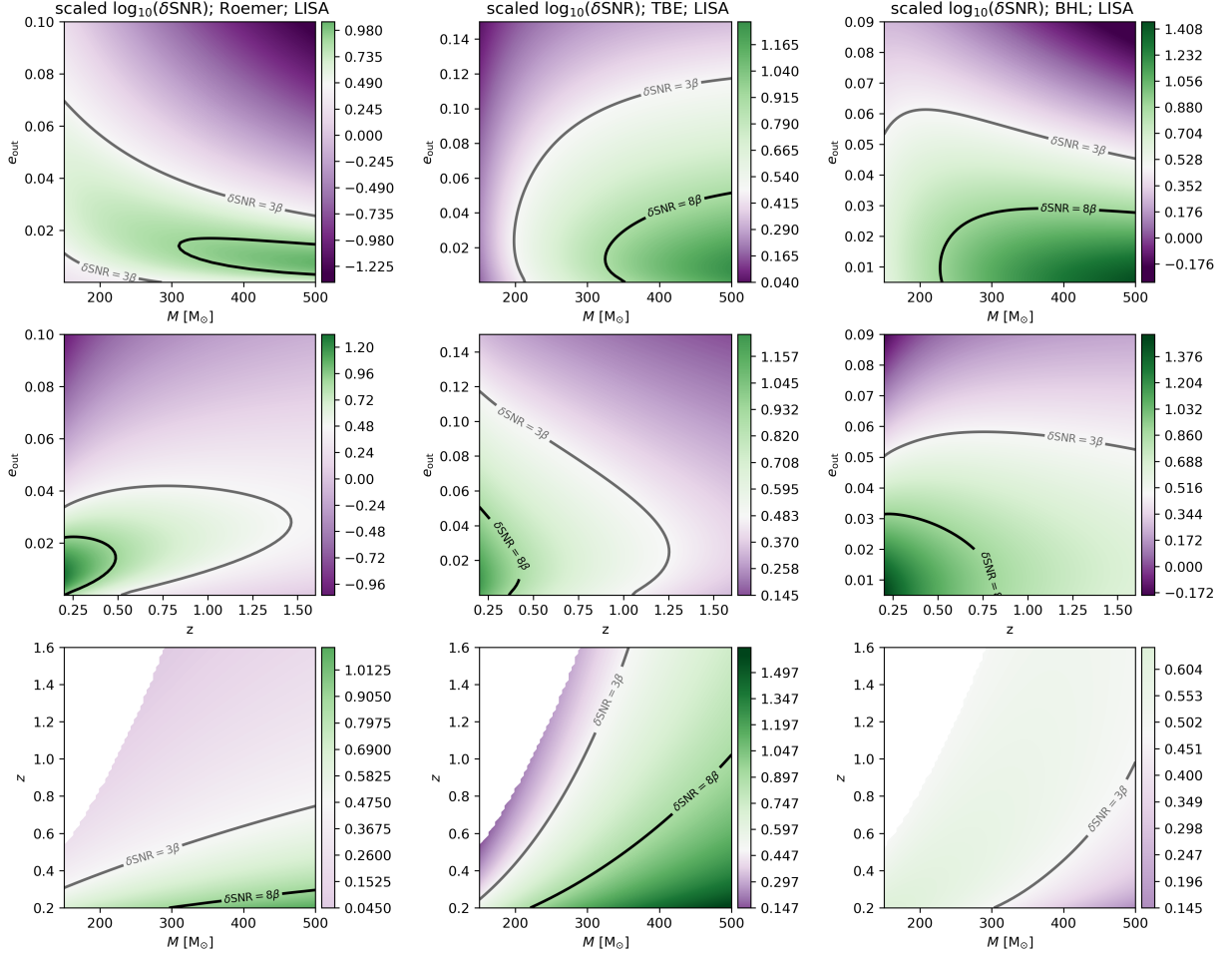


FIG. 8. Two dimensional slices of the δSNR cubes for various dephasing prescriptions with a fixed value of the parameter ξ (for LISA). Note how the contours vary purely as a function of binary parameters. Green regions of phase space are more likely to present detectable EE, all else being equal.

- [7] M. Zevin, S. S. Bavera, C. P. L. Berry, V. Kalogera, T. Fragos, P. Marchant, C. L. Rodriguez, F. Antonini, D. E. Holz, and C. Pankow, One Channel to Rule Them All? Constraining the Origins of Binary Black Holes Using Multiple Formation Pathways, *Astrophys. J.* **910**, 152 (2021), [arXiv:2011.10057 \[astro-ph.HE\]](#).
- [8] M. Zevin, S. S. Bavera, C. P. L. Berry, V. Kalogera, T. Fragos, P. Marchant, C. L. Rodriguez, F. Antonini, D. E. Holz, and C. Pankow, One Channel to Rule Them All? Constraining the Origins of Binary Black Holes Using Multiple Formation Pathways, *Astrophys. J.* **910**, 152 (2021), [arXiv:2011.10057 \[astro-ph.HE\]](#).
- [9] C. Kimball, C. Talbot, C. P. L. Berry, M. Zevin, E. Thrane, V. Kalogera, R. Busicchio, M. Carney, T. Dent, H. Middleton, E. Payne, J. Veitch, and D. Williams, Evidence for Hierarchical Black Hole Mergers in the Second LIGO-Virgo Gravitational Wave Catalog, *ApJ* **915**, L35 (2021), [arXiv:2011.05332 \[astro-ph.HE\]](#).
- [10] A. Santini, D. Gerosa, R. Cotesta, and E. Berti, Black-hole mergers in disklike environments could explain the observed $q-\chi_{eff}$ correlation, *Phys. Rev. D* **108**, 083033 (2023), [arXiv:2308.12998 \[astro-ph.HE\]](#).
- [11] K. Gültekin, M. C. Miller, and D. P. Hamilton, Three-Body Dynamics with Gravitational Wave Emission, *Astrophys. J.* **640**, 156 (2006).
- [12] J. Samsing, M. MacLeod, and E. Ramirez-Ruiz, The Formation of Eccentric Compact Binary Inspirals and the Role of Gravitational Wave Emission in Binary-Single Stellar Encounters, *Astrophys. J.* **784**, 71 (2014), [arXiv:1308.2964 \[astro-ph.HE\]](#).
- [13] J. Samsing and E. Ramirez-Ruiz, On the Assembly Rate of Highly Eccentric Binary Black Hole Mergers, *ApJ* **840**, L14 (2017), [arXiv:1703.09703 \[astro-ph.HE\]](#).
- [14] J. Samsing and T. Ilan, Topology of black hole binary-single interactions, *MNRAS* **476**, 1548 (2018), [arXiv:1706.04672 \[astro-ph.HE\]](#).
- [15] J. Samsing, M. MacLeod, and E. Ramirez-Ruiz, Dissipative Evolution of Unequal-mass Binary-single Interactions and Its Relevance to Gravitational-wave Detections, *Astrophys. J.* **853**, 140 (2018), [arXiv:1706.03776 \[astro-ph.HE\]](#).
- [16] J. Samsing, Eccentric black hole mergers forming in globular clusters, *Phys. Rev. D* **97**, 103014 (2018), [arXiv:1711.07452 \[astro-ph.HE\]](#).

- [17] J. Takátsy, B. Bécsy, and P. Raffai, Eccentricity distributions of eccentric binary black holes in galactic nuclei, *Mon. Not. Roy. Astron. Soc.* **486**, 570 (2019), [arXiv:1812.04012 \[astro-ph.HE\]](#).
- [18] J. Samsing, A. Askar, and M. Giersz, MOCCA-SURVEY Database. I. Eccentric Black Hole Mergers during Binary-Single Interactions in Globular Clusters, *Astrophys. J.* **855**, 124 (2018), [arXiv:1712.06186 \[astro-ph.HE\]](#).
- [19] J. Samsing and D. J. D’Orazio, Black Hole Mergers From Globular Clusters Observable by LISA I: Eccentric Sources Originating From Relativistic N-body Dynamics, *MNRAS* **10.1093/mnras/sty2334** (2018), [arXiv:1804.06519 \[astro-ph.HE\]](#).
- [20] C. L. Rodriguez, P. Amaro-Seoane, S. Chatterjee, K. Kremer, F. A. Rasio, J. Samsing, C. S. Ye, and M. Zevin, Post-Newtonian dynamics in dense star clusters: Formation, masses, and merger rates of highly-eccentric black hole binaries, *Phys. Rev. D* **98**, 123005 (2018), [arXiv:1811.04926 \[astro-ph.HE\]](#).
- [21] B. Liu, D. Lai, and Y.-H. Wang, Black Hole and Neutron Star Binary Mergers in Triple Systems. II. Merger Eccentricity and Spin-Orbit Misalignment, *Astrophys. J.* **881**, 41 (2019), [arXiv:1905.00427 \[astro-ph.HE\]](#).
- [22] M. Zevin, J. Samsing, C. Rodriguez, C.-J. Haster, and E. Ramirez-Ruiz, Eccentric Black Hole Mergers in Dense Star Clusters: The Role of Binary-Binary Encounters, *Astrophys. J.* **871**, 91 (2019), [arXiv:1810.00901 \[astro-ph.HE\]](#).
- [23] J. Samsing, A. S. Hamers, and J. G. Tyles, Effect of distant encounters on black hole binaries in globular clusters: Systematic increase of in-cluster mergers in the LISA band, *Phys. Rev. D* **100**, 043010 (2019), [arXiv:1906.07189 \[astro-ph.HE\]](#).
- [24] J. Samsing, D. J. D’Orazio, K. Kremer, C. L. Rodriguez, and A. Askar, Single-single gravitational-wave captures in globular clusters: Eccentric deci-Hertz sources observable by DECIGO and Tian-Qin, *Phys. Rev. D* **101**, 123010 (2020), [arXiv:1907.11231 \[astro-ph.HE\]](#).
- [25] A. A. Trani, N. W. C. Leigh, T. C. N. Boekholt, and S. Portegies Zwart, Isles of regularity in a sea of chaos amid the gravitational three-body problem, *A&A* **689**, A24 (2024), [arXiv:2403.03247 \[astro-ph.EP\]](#).
- [26] J. Samsing, M. MacLeod, and E. Ramirez-Ruiz, The Formation of Eccentric Compact Binary Inspirals and the Role of Gravitational Wave Emission in Binary-Single Stellar Encounters, *Astrophys. J.* **784**, 71 (2014), [arXiv:1308.2964 \[astro-ph.HE\]](#).
- [27] J. Samsing, Eccentric black hole mergers forming in globular clusters, *Phys. Rev. D* **97**, 103014 (2018), [arXiv:1711.07452 \[astro-ph.HE\]](#).
- [28] M. Zevin, C. Pankow, C. L. Rodriguez, L. Sampson, E. Chase, V. Kalogera, and F. A. Rasio, Constraining Formation Models of Binary Black Holes with Gravitational-wave Observations, *Astrophys. J.* **846**, 82 (2017), [arXiv:1704.07379 \[astro-ph.HE\]](#).
- [29] M. Zevin, J. Samsing, C. Rodriguez, C.-J. Haster, and E. Ramirez-Ruiz, Eccentric Black Hole Mergers in Dense Star Clusters: The Role of Binary-Binary Encounters, *Astrophys. J.* **871**, 91 (2019), [arXiv:1810.00901 \[astro-ph.HE\]](#).
- [30] S. K. Chakrabarti, Binary Black Holes in Stationary Orbits and a Test of the Active Galactic Nucleus Paradigm, *Astrophys. J.* **411**, 610 (1993).
- [31] F. D. Ryan, Gravitational waves from the inspiral of a compact object into a massive, axisymmetric body with arbitrary multipole moments, *Phys. Rev. D* **52**, 5707 (1995).
- [32] E. Barausse and L. Rezzolla, Influence of the hydrodynamic drag from an accretion torus on extreme mass-ratio inspirals, *Phys. Rev. D* **77**, 104027 (2008), [arXiv:0711.4558 \[gr-qc\]](#).
- [33] Y. Levin, Starbursts near supermassive black holes: young stars in the Galactic Centre, and gravitational waves in LISA band, *MNRAS* **374**, 515 (2007), [arXiv:astro-ph/0603583 \[astro-ph\]](#).
- [34] B. Kocsis, N. Yunes, and A. Loeb, Observable signatures of extreme mass-ratio inspiral black hole binaries embedded in thin accretion disks, *Phys. Rev. D* **84**, 024032 (2011), [arXiv:1104.2322 \[astro-ph.GA\]](#).
- [35] E. Barausse, V. Cardoso, and P. Pani, Can environmental effects spoil precision gravitational-wave astrophysics?, *Phys. Rev. D* **89**, 104059 (2014), [arXiv:1404.7149 \[gr-qc\]](#).
- [36] K. Inayoshi, R. Hirai, T. Kinugawa, and K. Hotokezaka, Formation pathway of Population III coalescing binary black holes through stable mass transfer, *MNRAS* **468**, 5020 (2017), [arXiv:1701.04823 \[astro-ph.HE\]](#).
- [37] Y. Meiron, B. Kocsis, and A. Loeb, Detecting Triple Systems with Gravitational Wave Observations, *Astrophys. J.* **834**, 200 (2017), [arXiv:1604.02148 \[astro-ph.HE\]](#).
- [38] M. Bonetti, E. Barausse, G. Faye, F. Haardt, and A. Sesana, About gravitational-wave generation by a three-body system, *Classical and Quantum Gravity* **34**, 215004 (2017), [arXiv:1707.04902 \[gr-qc\]](#).
- [39] A. Torres-Orjuela, X. Chen, Z. Cao, P. Amaro-Seoane, and P. Peng, Detecting the beaming effect of gravitational waves, *Phys. Rev. D* **100**, 063012 (2019), [arXiv:1806.09857 \[astro-ph.HE\]](#).
- [40] L. Randall and Z.-Z. Xianyu, Observing Eccentricity Oscillations of Binary Black Holes in LISA, *arXiv e-prints*, [arXiv:1902.08604](#) (2019), [arXiv:1902.08604 \[astro-ph.HE\]](#).
- [41] V. Cardoso and A. Maselli, Constraints on the astrophysical environment of binaries with gravitational-wave observations, *A&A* **644**, A147 (2020), [arXiv:1909.05870 \[astro-ph.HE\]](#).
- [42] D. J. D’Orazio and A. Loeb, Repeated gravitational lensing of gravitational waves in hierarchical black hole triples, *Phys. Rev. D* **101**, 083031 (2020), [arXiv:1910.02966 \[astro-ph.HE\]](#).
- [43] B. Liu, D. J. D’Orazio, A. Vigna-Gómez, and J. Samsing, Uncovering a hidden black hole binary from secular eccentricity variations of a tertiary star, *Phys. Rev. D* **106**, 123010 (2022), [arXiv:2207.10091 \[astro-ph.HE\]](#).
- [44] Z. Xuan, S. Naoz, and X. Chen, Detecting Accelerating Eccentric Binaries in the LISA Band, *arXiv e-prints*, [arXiv:2210.03129](#) (2022), [arXiv:2210.03129 \[astro-ph.HE\]](#).
- [45] M. Garg, A. Derdzinski, L. Zwick, P. R. Capelo, and L. Mayer, The imprint of gas on gravitational waves from LISA intermediate-mass black hole binaries, *MNRAS* **517**, 1339 (2022), [arXiv:2206.05292 \[astro-ph.GA\]](#).
- [46] P. S. Cole, A. Coogan, B. J. Kavanagh, and G. Bertone, Measuring dark matter spikes around primordial black holes with Einstein Telescope and Cosmic Explorer, *arXiv e-prints*, [arXiv:2207.07576](#) (2022),

- [arXiv:2207.07576 \[astro-ph.CO\]](#).
- [47] R. S. Chandramouli and N. Yunes, Ready-to-use analytic model for gravitational waves from a hierarchical triple with Kozai-Lidov oscillations, *Phys. Rev. D* **105**, 064009 (2022), [arXiv:2107.00741 \[gr-qc\]](#).
- [48] L. Sberna, S. Babak, S. Marsat, A. Caputo, G. Cusin, A. Toubiana, E. Barausse, C. Caprini, T. Dal Canton, A. Sesana, and N. Tamanini, Observing GW190521-like binary black holes and their environment with LISA, *Phys. Rev. D* **106**, 064056 (2022), [arXiv:2205.08550 \[gr-qc\]](#).
- [49] L. Zwick, P. R. Capelo, and L. Mayer, Priorities in gravitational waveforms for future space-borne detectors: vacuum accuracy or environment?, *MNRAS* **521**, 4645 (2023), [arXiv:2209.04060 \[gr-qc\]](#).
- [50] C. Tiede, D. J. D’Orazio, L. Zwick, and P. C. Duffell, Disk-induced Binary Precession: Implications for Dynamics and Multimessenger Observations of Black Hole Binaries, *Astrophys. J.* **964**, 46 (2024), [arXiv:2312.01805 \[astro-ph.HE\]](#).
- [51] C. Dyson, J. Redondo-Yuste, M. van de Meent, and V. Cardoso, Relativistic aerodynamics of spinning black holes, *Phys. Rev. D* **109**, 104038 (2024), [arXiv:2402.07981 \[gr-qc\]](#).
- [52] K. Destounis, A. Kulathingal, K. D. Kokkotas, and G. O. Papadopoulos, Gravitational-wave imprints of compact and galactic-scale environments in extreme-mass-ratio binaries, [arXiv e-prints](#), [arXiv:2210.09357 \(2022\)](#), [arXiv:2210.09357 \[gr-qc\]](#).
- [53] V. Cardoso, K. Destounis, F. Duque, R. P. Macedo, and A. Maselli, Gravitational Waves from Extreme-Mass-Ratio Systems in Astrophysical Environments, *Phys. Rev. Lett.* **129**, 241103 (2022), [arXiv:2210.01133 \[gr-qc\]](#).
- [54] A. Caputo, L. Sberna, A. Toubiana, S. Babak, E. Barausse, S. Marsat, and P. Pani, Gravitational-wave Detection and Parameter Estimation for Accreting Black-hole Binaries and Their Electromagnetic Counterpart, *Astrophys. J.* **892**, 90 (2020), [arXiv:2001.03620 \[astro-ph.HE\]](#).
- [55] L. Zwick, C. Tiede, A. A. Trani, A. Derdzinski, Z. Haiman, D. J. D’Orazio, and J. Samsing, Novel category of environmental effects on gravitational waves from binaries perturbed by periodic forces, *Phys. Rev. D* **110**, 103005 (2024), [arXiv:2405.05698 \[gr-qc\]](#).
- [56] A. Derdzinski, D. D’Orazio, P. Duffell, Z. Haiman, and A. MacFadyen, Evolution of gas disc-embedded intermediate mass ratio inspirals in the LISA band, *MNRAS* **501**, 3540 (2021), [arXiv:2005.11333 \[astro-ph.HE\]](#).
- [57] P. Basu, S. Chatterjee, and S. Mondal, Eccentric orbits in disc-embedded EMRIs : orbital evolution and observability trend in LISA, *MNRAS* **531**, 1506 (2024).
- [58] G. Caneva Santoro, S. Roy, R. Vicente, M. Haney, O. J. Piccinni, W. Del Pozzo, and M. Martinez, First Constraints on Compact Binary Environments from LIGO-Virgo Data, *Phys. Rev. Lett.* **132**, 251401 (2024), [arXiv:2309.05061 \[gr-qc\]](#).
- [59] J. I. Thorpe, J. Ziemer, I. Thorpe, J. Livas, J. W. Conklin, R. Caldwell, E. Berti, S. T. McWilliams, R. Stebbins, D. Shoemaker, E. C. Ferrara, S. L. Larson, D. Shoemaker, J. S. Key, M. Vallisneri, M. Eracleous, J. Schnittman, B. Kamai, J. Camp, G. Mueller, J. Bellovary, N. Rioux, J. Baker, P. L. Bender, C. Cutler, N. Cornish, C. Hogan, S. Manthripragada, B. Ware, P. Natarajan, K. Numata, S. R. Sankar, B. J. Kelly, K. McKenzie, J. Slutsky, R. Spero, M. Hewitson, S. Francis, R. DeRosa, A. Yu, A. Hornschemeier, and P. Wass, The Laser Interferometer Space Antenna: Unveiling the Millihertz Gravitational Wave Sky, in *Bulletin of the American Astronomical Society*, Vol. 51 (2019) p. 77, [arXiv:1907.06482 \[astro-ph.IM\]](#).
- [60] M. Colpi, K. Danzmann, M. Hewitson, K. Holley-Bockelmann, P. Jetzer, G. Nelemans, A. Petiteau, D. Shoemaker, C. Sopena, R. Stebbins, N. Tanvir, H. Ward, W. J. Weber, I. Thorpe, A. Dauriskikh, A. Deep, I. Fernández Núñez, C. García Marirrodiga, M. Gehler, J.-P. Halain, O. Jennrich, U. Lammers, J. Larrañaga, M. Lieser, N. Lützgendorf, W. Martens, L. Mondin, A. Piris Niño, P. Amaro-Seoane, M. Arca Sedda, P. Auclair, S. Babak, Q. Baghi, V. Baibhav, T. Baker, J.-B. Bayle, C. Berry, E. Berti, G. Boileau, M. Bonetti, R. Brito, R. Busicchio, G. Calcagni, P. R. Capelo, C. Caprini, A. Caputo, E. Castelli, H.-Y. Chen, X. Chen, A. Chua, G. Davies, A. Derdzinski, V. F. Domcke, D. Doneva, I. Dvorkin, J. María Ezquiaga, J. Gair, Z. Haiman, I. Harry, O. Hartwig, A. Hees, A. Hefernan, S. Husa, D. Izquierdo, N. Karnesis, A. Klein, V. Korol, N. Korsakova, T. Kupfer, D. Laghi, A. Lamberts, S. Larson, M. Le Jeune, M. Lewicki, T. Littenberg, E. Madge, A. Mangiagli, S. Marsat, I. M. Vilchez, A. Maselli, J. Mathews, M. van de Meent, M. Muratore, G. Nardini, P. Pani, M. Peloso, M. Pieroni, A. Pound, H. Quelquejay-Leclere, A. Ricciardone, E. M. Rossi, A. Sartirana, E. Savalle, L. Sberna, A. Sesana, D. Shoemaker, J. Slutsky, T. Sotiriou, L. Speri, M. Staab, D. Steer, N. Tamanini, G. Tasinato, J. Torrado, A. Torres-Orjuela, A. Toubiana, M. Vallisneri, A. Vecchio, M. Volonteri, K. Yagi, and L. Zwick, LISA Definition Study Report, [arXiv e-prints](#), [arXiv:2402.07571 \(2024\)](#), [arXiv:2402.07571 \[astro-ph.CO\]](#).
- [61] J. Samsing, K. Hendriks, L. Zwick, D. J. D’Orazio, and B. Liu, Gravitational Wave Phase Shifts in Eccentric Black Hole Mergers as a Probe of Dynamical Formation Environments, [arXiv e-prints](#), [arXiv:2403.05625 \(2024\)](#), [arXiv:2403.05625 \[astro-ph.HE\]](#).
- [62] K. Hendriks, D. Atallah, M. Martinez, M. Zevin, L. Zwick, A. A. Trani, P. Saini, J. Takátsy, and J. Samsing, Large Gravitational Wave Phase Shifts from Strong 3-body Interactions in Dense Stellar Clusters, [arXiv e-prints](#), [arXiv:2411.08572 \(2024\)](#), [arXiv:2411.08572 \[astro-ph.HE\]](#).
- [63] K. Hendriks, L. Zwick, and J. Samsing, Eccentric features in the gravitational wave phase of dynamically formed black hole binaries, [arXiv e-prints](#), [arXiv:2408.04603 \(2024\)](#), [arXiv:2408.04603 \[gr-qc\]](#).
- [64] T. Robson, N. J. Cornish, N. Tamanini, and S. Toonen, Detecting hierarchical stellar systems with LISA, *Phys. Rev. D* **98**, 064012 (2018), [arXiv:1806.00500 \[gr-qc\]](#).
- [65] B. Liu, D. J. Muñoz, and D. Lai, Suppression of extreme orbital evolution in triple systems with short-range forces, *MNRAS* **447**, 747 (2015), [arXiv:1409.6717 \[astro-ph.EP\]](#).
- [66] A. Toubiana, L. Sberna, A. Caputo, G. Cusin, S. Marsat, K. Jani, S. Babak, E. Barausse, C. Caprini, P. Pani, A. Sesana, and N. Tamanini, Detectable Environmental Effects in GW190521-like Black-Hole Binaries with LISA, *Phys. Rev. Lett.* **126**, 101105 (2021), [arXiv:2010.06056 \[astro-ph.HE\]](#).

- [67] M. Martin Barandiaran, S. Kuroyanagi, and S. Nesseris, Gravitational waves in the circular restricted three body problem, *Classical and Quantum Gravity* **41**, 095002 (2024), [arXiv:2309.15510 \[gr-qc\]](#).
- [68] L. Zwick, C. Tiede, A. A. Trani, A. Derdzinski, Z. Haiman, D. J. D’Orazio, and J. Samsing, Novel category of environmental effects on gravitational waves from binaries perturbed by periodic forces, *Phys. Rev. D* **110**, 103005 (2024), [arXiv:2405.05698 \[gr-qc\]](#).
- [69] L. Speri, A. Antonelli, L. Sberna, S. Babak, E. Barausse, J. R. Gair, and M. L. Katz, Measuring accretion-disk effects with gravitational waves from extreme mass ratio inspirals, *arXiv e-prints*, [arXiv:2207.10086 \(2022\)](#), [arXiv:2207.10086 \[gr-qc\]](#).
- [70] F. Duque, S. Kejriwal, L. Sberna, L. Speri, and J. Gair, Constraining accretion physics with gravitational waves from eccentric extreme-mass-ratio inspirals, *arXiv e-prints*, [arXiv:2411.03436 \(2024\)](#), [arXiv:2411.03436 \[gr-qc\]](#).
- [71] I. Romero-Shaw, P. D. Lasky, E. Thrane, and J. Calderón Bustillo, GW190521: Orbital Eccentricity and Signatures of Dynamical Formation in a Binary Black Hole Merger Signal, *ApJ* **903**, L5 (2020), [arXiv:2009.04771 \[astro-ph.HE\]](#).
- [72] A. A. Trani, S. Rastello, U. N. D. Carlo, F. Santoliquido, A. Tanikawa, and M. Mapelli, Compact object mergers in hierarchical triples from low-mass young star clusters, *MNRAS* **10.1093/mnras/stac122** (2022), [arXiv:2111.06388 \[astro-ph.HE\]](#).
- [73] J. Samsing, I. Bartos, D. J. D’Orazio, Z. Haiman, B. Kocsis, N. W. C. Leigh, B. Liu, M. E. Pessah, and H. Tagawa, AGN as potential factories for eccentric black hole mergers, *Nature (London)* **603**, 237 (2022).
- [74] A. A. Trani, S. Quaini, and M. Colpi, Three-body encounters in black hole discs around a supermassive black hole. The disc velocity dispersion and the Keplerian tidal field determine the eccentricity and spin-orbit alignment of gravitational wave mergers, *A&A* **683**, A135 (2024), [arXiv:2312.13281 \[astro-ph.HE\]](#).
- [75] A. A. Trani, N. W. C. Leigh, T. C. N. Boekholt, and S. Portegies Zwart, Isles of regularity in a sea of chaos amid the gravitational three-body problem, *A&A* **689**, A24 (2024), [arXiv:2403.03247 \[astro-ph.EP\]](#).
- [76] D. Marín Pina, M. Gieles, T. Andrade, and A. A. Trani, Interactions among binary black holes in star clusters: eccentric gravitational wave captures and triple formation, *arXiv e-prints*, [arXiv:2501.02907 \(2025\)](#), [arXiv:2501.02907 \[astro-ph.GA\]](#).
- [77] J. Stegmann, A. Vigna-Gómez, A. Rantala, T. Wagg, L. Zwick, M. Renzo, L. A. C. van Son, S. E. de Mink, and S. D. M. White, Close Encounters of Wide Binaries Induced by the Galactic Tide: Implications for Stellar Mergers and Gravitational-wave Sources, *ApJ* **972**, L19 (2024), [arXiv:2405.02912 \[astro-ph.GA\]](#).
- [78] P. C. Peters, Gravitational Radiation and the Motion of Two Point Masses, *Physical Review* **136**, 1224 (1964).
- [79] S. F. Portegies Zwart and S. L. W. McMillan, Black Hole Mergers in the Universe, *Astrophys. J.* **528**, L17 (2000).
- [80] W. H. Lee, E. Ramirez-Ruiz, and G. van de Ven, SHORT GAMMA-RAY BURSTS FROM DYNAMICALLY ASSEMBLED COMPACT BINARIES IN GLOBULAR CLUSTERS: PATHWAYS, RATES, HYDRODYNAMICS, AND COSMOLOGICAL SETTING, *Astrophys. J.* **720**, 953 (2010).
- [81] S. Banerjee, H. Baumgardt, and P. Kroupa, Stellar-mass black holes in star clusters: implications for gravitational wave radiation, *MNRAS* **402**, 371 (2010), [arXiv:0910.3954 \[astro-ph.SR\]](#).
- [82] A. Tanikawa, Dynamical evolution of stellar mass black holes in dense stellar clusters: estimate for merger rate of binary black holes originating from globular clusters, *MNRAS* **435**, 1358 (2013), [arXiv:1307.6268](#).
- [83] Y.-B. Bae, C. Kim, and H. M. Lee, Compact binaries ejected from globular clusters as gravitational wave sources, *MNRAS* **440**, 2714 (2014), [arXiv:1308.1641 \[astro-ph.HE\]](#).
- [84] C. L. Rodriguez, M. Morscher, B. Pattabiraman, S. Chatterjee, C.-J. Haster, and F. A. Rasio, Binary Black Hole Mergers from Globular Clusters: Implications for Advanced LIGO, *Phys. Rev. Lett.* **115**, 051101 (2015), [arXiv:1505.00792 \[astro-ph.HE\]](#).
- [85] E. Ramirez-Ruiz, M. Trenti, M. MacLeod, L. F. Roberts, W. H. Lee, and M. I. Saladino-Rosas, Compact Stellar Binary Assembly in the First Nuclear Star Clusters and r-process Synthesis in the Early Universe, *ApJ* **802**, L22 (2015), [arXiv:1410.3467](#).
- [86] C. L. Rodriguez, S. Chatterjee, and F. A. Rasio, Binary black hole mergers from globular clusters: Masses, merger rates, and the impact of stellar evolution, *Phys. Rev. D* **93**, 084029 (2016), [arXiv:1602.02444 \[astro-ph.HE\]](#).
- [87] C. L. Rodriguez, C.-J. Haster, S. Chatterjee, V. Kalogera, and F. A. Rasio, Dynamical Formation of the GW150914 Binary Black Hole, *ApJ* **824**, L8 (2016), [arXiv:1604.04254 \[astro-ph.HE\]](#).
- [88] A. Askar, M. Szkudlarek, D. Gondek-Rosińska, M. Giersz, and T. Bulik, MOCCA-SURVEY Database - I. Coalescing binary black holes originating from globular clusters, *MNRAS* **464**, L36 (2017), [arXiv:1608.02520 \[astro-ph.HE\]](#).
- [89] D. Park, C. Kim, H. M. Lee, Y.-B. Bae, and K. Belczynski, Black hole binaries dynamically formed in globular clusters, *MNRAS* **469**, 4665 (2017), [arXiv:1703.01568 \[astro-ph.HE\]](#).
- [90] A. A. Trani, A. Tanikawa, M. S. Fujii, N. W. C. Leigh, and J. Kumamoto, Spin misalignment of black hole binaries from young star clusters: implications for the origin of gravitational waves events, *MNRAS* **504**, 910 (2021), [arXiv:2102.01689 \[astro-ph.HE\]](#).
- [91] S. Naoz, B. Kocsis, A. Loeb, and N. Yunes, Resonant Post-Newtonian Eccentricity Excitation in Hierarchical Three-body Systems, *Astrophys. J.* **773**, 187 (2013), [arXiv:1206.4316 \[astro-ph.SR\]](#).
- [92] G. Li, S. Naoz, B. Kocsis, and A. Loeb, Eccentricity Growth and Orbit Flip in Near-coplanar Hierarchical Three-body Systems, *Astrophys. J.* **785**, 116 (2014), [arXiv:1310.6044 \[astro-ph.EP\]](#).
- [93] F. Antonini, S. Chatterjee, C. L. Rodriguez, M. Morscher, B. Pattabiraman, V. Kalogera, and F. A. Rasio, Black Hole Mergers and Blue Stragglers from Hierarchical Triples Formed in Globular Clusters, *Astrophys. J.* **816**, 65 (2016), [arXiv:1509.05080](#).
- [94] J. M. O. Antognini and T. A. Thompson, Dynamical formation and scattering of hierarchical triples: cross-sections, Kozai-Lidov oscillations, and collisions, *MNRAS* **456**, 4219 (2016), [arXiv:1507.03593 \[astro-ph.SR\]](#).

- [95] K. Silsbee and S. Tremaine, Lidov-Kozai Cycles with Gravitational Radiation: Merging Black Holes in Isolated Triple Systems, *Astrophys. J.* **836**, 39 (2017), [arXiv:1608.07642 \[astro-ph.HE\]](#).
- [96] L. Randall and Z.-Z. Xianyu, An Analytical Portrait of Binary Mergers in Hierarchical Triple Systems, *Astrophys. J.* **864**, 134 (2018), [arXiv:1802.05718 \[gr-qc\]](#).
- [97] A. S. Hamers and T. A. Thompson, Double Neutron Star Mergers from Hierarchical Triple-star Systems, *Astrophys. J.* **883**, 23 (2019), [arXiv:1907.08297 \[astro-ph.HE\]](#).
- [98] B. Liu and D. Lai, Hierarchical black hole mergers in multiple systems: constrain the formation of GW190412-, GW190814-, and GW190521-like events, *MNRAS* **502**, 2049 (2021), [arXiv:2009.10068 \[astro-ph.HE\]](#).
- [99] A. A. Trani, S. Rastello, U. N. Di Carlo, F. Santoliquido, A. Tanikawa, and M. Mapelli, Compact object mergers in hierarchical triples from low-mass young star clusters, *MNRAS* **511**, 1362 (2022), [arXiv:2111.06388 \[astro-ph.HE\]](#).
- [100] I. Bartos, B. Kocsis, Z. Haiman, and S. Márka, Rapid and Bright Stellar-mass Binary Black Hole Mergers in Active Galactic Nuclei, *Astrophys. J.* **835**, 165 (2017), [arXiv:1602.03831 \[astro-ph.HE\]](#).
- [101] N. C. Stone, B. D. Metzger, and Z. Haiman, Assisted inspirals of stellar mass black holes embedded in AGN discs: solving the ‘final au problem’, *MNRAS* **464**, 946 (2017), [arXiv:1602.04226](#).
- [102] B. McKernan, K. E. S. Ford, J. Bellovary, N. W. C. Leigh, Z. Haiman, B. Kocsis, W. Lyra, M.-M. MacLow, B. Metzger, M. O’Dowd, S. Endlich, and D. J. Rosen, On stellar-mass black hole mergers in AGN disks detectable with LIGO, *ArXiv e-prints* (2017), [arXiv:1702.07818 \[astro-ph.HE\]](#).
- [103] H. Tagawa, Z. Haiman, and B. Kocsis, Formation and Evolution of Compact-object Binaries in AGN Disks, *Astrophys. J.* **898**, 25 (2020), [arXiv:1912.08218 \[astro-ph.GA\]](#).
- [104] J. Samsing, I. Bartos, D. J. D’Orazio, Z. Haiman, B. Kocsis, N. W. C. Leigh, B. Liu, M. E. Pessah, and H. Tagawa, AGN as potential factories for eccentric black hole mergers, *Nature (London)* **603**, 237 (2022), [arXiv:2010.09765 \[astro-ph.HE\]](#).
- [105] A. A. Trani, S. Quaini, and M. Colpi, Three-body encounters in black hole discs around a supermassive black hole: The disc velocity dispersion and the Keplerian tidal field determine the eccentricity and spin-orbit alignment of gravitational wave mergers, *arXiv e-prints*, [arXiv:2312.13281 \(2023\)](#), [arXiv:2312.13281 \[astro-ph.HE\]](#).
- [106] G. Fabj and J. Samsing, Eccentric mergers in agn discs: Influence of the supermassive black-hole on three-body interactions, *arXiv e-prints*, [arXiv:2402.16948 \(2024\)](#).
- [107] C. Cahillane and G. Mansell, Review of the Advanced LIGO Gravitational Wave Observatories Leading to Observing Run Four, *Galaxies* **10**, 36 (2022), [arXiv:2202.00847 \[gr-qc\]](#).
- [108] E. Capote, W. Jia, N. Aritomi, M. Nakano, V. Xu, R. Abbott, I. Abouelfettouh, R. X. Adhikari, A. Ananyeva, S. Appert, S. K. Apple, K. Arai, S. M. Aston, M. Ball, S. W. Ballmer, D. Barker, L. Barsotti, B. K. Berger, J. Betzwieser, D. Bhattacharjee, G. Billingsley, S. Biscans, C. D. Blair, N. Bode, E. Bonilla, V. Bossilkov, A. Branch, A. F. Brooks, D. D. Brown, J. Bryant, C. Cahillane, H. Cao, F. Clara, J. Collins, C. M. Compton, R. Cottingham, D. C. Coyne, R. Crouch, J. Csizmazia, A. Cumming, L. P. Dartez, D. Davis, N. Demos, E. Dohmen, J. C. Driggers, S. E. Dwyer, A. Effler, A. Ejlli, T. Etzel, M. Evans, J. Feicht, R. Frey, W. Frischhertz, P. Fritschel, V. V. Frolov, M. Fuentes-Garcia, P. Fulda, M. Fyffe, D. Ganapathy, B. Gateley, T. Gayer, J. A. Giaime, K. D. Giardina, J. Glanzer, E. Goetz, R. Goetz, A. W. Goodwin-Jones, S. Gras, C. Gray, D. Griffith, H. Grote, T. Guidry, J. Gurs, E. D. Hall, J. Hanks, J. Hanson, M. C. Heintze, A. F. Helmling-Cornell, N. A. Holland, D. Hoyland, H. Y. Huang, Y. Inoue, A. L. James, A. Jamies, A. Jennings, D. H. Jones, H. B. Kabagoz, S. Karat, S. Karki, M. Kasprzack, K. Kawabe, N. Kijbunchoo, P. J. King, J. S. Kissel, K. Komori, A. Kontos, R. Kumar, K. Kuns, M. Landry, B. Lantz, M. Laxen, K. Lee, M. Lesovsky, F. L. Villarreal, M. Lormand, H. A. Loughlin, R. Macas, M. MacInnis, C. N. Makarem, B. Mannix, G. L. Mansell, R. M. Martin, K. Mason, F. Matichard, N. Mavalvala, N. Maxwell, G. McCarrol, R. McCarthy, D. E. McClelland, S. McCormick, T. McRae, F. Mera, E. L. Merill, F. Meylahn, R. Mittleman, D. Moraru, G. Moreno, A. Mullavey, T. J. N. Nelson, A. Neunzert, J. Notte, J. Oberling, T. O’Hanlon, C. Osthelder, D. J. Ottaway, H. Overmier, W. Parker, O. Patane, A. Pele, H. Pham, M. Pirello, J. Pullin, V. Quetschke, K. E. Ramirez, K. Ransom, J. Reyes, J. W. Richardson, M. Robinson, J. G. Rollins, C. L. Romel, J. H. Romie, M. P. Ross, K. Ryan, T. Sadecki, A. Sanchez, E. J. Sanchez, L. E. Sanchez, R. L. Savage, D. Schaetzl, M. G. Schirowski, R. Schnabel, R. M. S. Schofield, E. Schwartz, D. Sellers, T. Shaffer, R. W. Short, D. Sigg, B. J. J. Slagmolen, C. Soike, S. Soni, V. Srivastava, L. Sun, D. B. Tanner, M. Thomas, P. Thomas, K. A. Thorne, M. R. Todd, C. I. Torrie, G. Traylor, A. S. Ubhi, G. Vajente, J. Vanosky, A. Vecchio, P. J. Veitch, A. M. Vibhute, E. R. G. von Reis, J. Warner, B. Weaver, R. Weiss, C. Whittle, B. Willke, C. C. Wipf, J. L. Wright, H. Yamamoto, L. Zhang, and M. E. Zucker, Advanced LIGO detector performance in the fourth observing run, *Phys. Rev. D* **111**, 062002 (2025), [arXiv:2411.14607 \[gr-qc\]](#).
- [109] I. Gupta, C. Afle, K. G. Arun, A. Bandopadhyay, M. Baryakhtar, S. Biscoveanu, S. Borhanian, F. Broekgaard, A. Corsi, A. Dhani, M. Evans, E. D. Hall, O. A. Hannuksela, K. Kacanja, R. Kashyap, S. Khadkikar, K. Kuns, T. G. F. Li, A. L. Miller, A. Harvey Nitz, B. J. Owen, C. Palomba, A. Pearce, H. Phurailatpam, B. Rajbhandari, J. Read, J. D. Romano, B. S. Sathyaprakash, D. H. Shoemaker, D. Singh, S. Vitale, L. Barsotti, E. Berti, C. Cahillane, H.-Y. Chen, P. Fritschel, C.-J. Haster, P. Landry, G. Lovelace, D. McClelland, B. J. J. Slagmolen, J. R. Smith, M. Soares-Santos, L. Sun, D. Tanner, H. Yamamoto, and M. Zucker, Characterizing gravitational wave detector networks: from Ajinline-formula₁ to cosmic explorer, *Classical and Quantum Gravity* **41**, 245001 (2024), [arXiv:2307.10421 \[gr-qc\]](#).
- [110] M. Evans, A. Corsi, C. Afle, A. Ananyeva, K. G. Arun, S. Ballmer, A. Bandopadhyay, L. Barsotti, M. Baryakhtar, E. Berger, E. Berti, S. Biscoveanu, S. Borhanian, F. Broekgaard, D. A. Brown,

- C. Cahillane, L. Campbell, H.-Y. Chen, K. J. Daniel, A. Dhani, J. C. Driggers, A. Effler, R. Eisenstein, S. Fairhurst, J. Feicht, P. Fritschel, P. Fulda, I. Gupta, E. D. Hall, G. Hammond, O. A. Hannuksela, H. Hansen, C.-J. Haster, K. Kacanja, B. Kamai, R. Kashyap, J. Shapiro Key, S. Khadkikar, A. Kontos, K. Kuns, M. Landry, P. Landry, B. Lantz, T. G. F. Li, G. Lovelace, V. Mandic, G. L. Mansell, D. Martynov, L. McCuller, A. L. Miller, A. H. Nitz, B. J. Owen, C. Palomba, J. Read, H. Phurailatpam, S. Reddy, J. Richardson, J. Rollins, J. D. Romano, B. S. Sathyaprakash, R. Schofield, D. H. Shoemaker, D. Sigg, D. Singh, B. Slagmolen, P. Sledge, J. Smith, M. Soares-Santos, A. Strunk, L. Sun, D. Tanner, L. A. C. van Son, S. Vitale, B. Willke, H. Yamamoto, and M. Zucker, Cosmic Explorer: A Submission to the NSF MPSAC ngGW Subcommittee, [arXiv e-prints](#), [arXiv:2306.13745 \(2023\)](#), [arXiv:2306.13745 \[astro-ph.IM\]](#).
- [111] M. Maggiore, C. Van Den Broeck, N. Bartolo, E. Belgacem, D. Bertacca, M. A. Bizouard, M. Branchesi, S. Clesse, S. Foffa, J. García-Bellido, S. Grimm, J. Harms, T. Hinderer, S. Matarrese, C. Palomba, M. Peloso, A. Ricciardone, and M. Sakellariadou, Science case for the Einstein telescope, *J. Cosmology Astropart. Phys.* **2020**, 050 (2020), [arXiv:1912.02622 \[astro-ph.CO\]](#).
- [112] M. Maggiore, *Gravitational Waves: Volume 2: Astrophysics and Cosmology* (2018).
- [113] M. Garg, A. Derdzinski, S. Tiwari, J. Gair, and L. Mayer, Measuring eccentricity and gas-induced perturbation from gravitational waves of LISA massive black hole binaries, [arXiv e-prints](#), [arXiv:2402.14058 \(2024\)](#), [arXiv:2402.14058 \[astro-ph.GA\]](#).
- [114] S. Roy and R. Vicente, Compact Binary Coalescences in Dense Environments Can Pose as in Vacuum, [arXiv e-prints](#), [arXiv:2410.16388 \(2024\)](#), [arXiv:2410.16388 \[gr-qc\]](#).
- [115] C. Cutler and É. E. Flanagan, Gravitational waves from merging compact binaries: How accurately can one extract the binary's parameters from the inspiral waveform?, *Phys. Rev. D* **49**, 2658 (1994), [arXiv:gr-qc/9402014 \[gr-qc\]](#).
- [116] L. Blanchet, Gravitational Radiation from Post-Newtonian Sources and Inspiralling Compact Binaries, *Living Reviews in Relativity* **17**, 2 (2014), [arXiv:1310.1528 \[gr-qc\]](#).
- [117] T. Robson, N. J. Cornish, and C. Liu, The construction and use of LISA sensitivity curves, *Class. Quantum Gravity* **36**, 105011 (2019), [arXiv:1803.01944 \[astro-ph.HE\]](#).
- [118] J. R. Gair, M. Vallisneri, S. L. Larson, and J. G. Baker, Testing General Relativity with Low-Frequency, Space-Based Gravitational-Wave Detectors, *Living Rev. Relat.* **16**, 7 (2013), [arXiv:1212.5575 \[gr-qc\]](#).
- [119] L. Zwick, P. R. Capelo, E. Bortolas, L. Mayer, and P. Amaro-Seoane, Improved gravitational radiation time-scales: significance for LISA and LIGO-Virgo sources, *MNRAS* **495**, 2321 (2020), [arXiv:1911.06024 \[astro-ph.GA\]](#).
- [120] B. Moore, M. Favata, K. G. Arun, and C. K. Mishra, Gravitational-wave phasing for low-eccentricity inspiralling compact binaries to 3PN order, *Phys. Rev. D* **93**, 124061 (2016), [arXiv:1605.00304 \[gr-qc\]](#).
- [121] N. Yunes, K. G. Arun, E. Berti, and C. M. Will, Post-circular expansion of eccentric binary inspirals: Fourier-domain waveforms in the stationary phase approximation, *Phys. Rev. D* **80**, 084001 (2009), [arXiv:0906.0313 \[gr-qc\]](#).
- [122] V. De Luca, G. Franciolini, P. Pani, and A. Riotto, The Minimum Testable Abundance of Primordial Black Holes at Future Gravitational-Wave Detectors, [arXiv e-prints](#), [arXiv:2106.13769 \(2021\)](#), [arXiv:2106.13769 \[astro-ph.CO\]](#).
- [123] B. Carr, F. Kühnel, and M. Sandstad, Primordial black holes as dark matter, *Phys. Rev. D* **94**, 083504 (2016), [arXiv:1607.06077](#).
- [124] R. Abbott, T. D. Abbott, F. Acernese, K. Ackley, C. Adams, N. Adhikari, R. X. Adhikari, V. B. Adya, C. Affeldt, D. Agarwal, M. Agathos, K. Agatsuma, N. Aggarwal, O. D. Aguiar, L. Aiello, A. Ain, P. Ajith, T. Akutsu, P. F. de Alarcón, S. Akcay, S. Albanesi, A. Allocca, P. A. Altin, A. Amato, C. Anand, S. Anand, A. Ananyeva, S. B. Anderson, W. G. Anderson, M. Ando, T. Andrade, N. Andres, T. Andrić, S. V. Angelova, S. Ansoldi, J. M. Antelis, S. Antier, F. Antonini, S. Appert, K. Arai, K. Arai, Y. Arai, S. Araki, A. Araya, M. C. Araya, J. S. Areeda, M. Arène, N. Armitomi, N. Arnaud, M. Aroneti, S. M. Aronson, K. G. Arun, H. Asada, Y. Asali, G. Ashton, Y. Aso, M. Assisduo, S. M. Aston, P. Astone, F. Aubin, C. Austin, S. Babak, F. Badaracco, M. K. M. Bader, C. Badger, S. Bae, Y. Bae, A. M. Baer, S. Bagnasco, Y. Bai, L. Baiotti, J. Baird, R. Bajpai, M. Ball, G. Ballardín, S. W. Ballmer, A. Balsamo, G. Baltus, S. Banagiri, D. Bankar, J. C. Barayoga, C. Barbieri, B. C. Barish, D. Barker, P. Barneo, F. Barone, B. Barr, L. Barsotti, M. Barsuglia, D. Barta, J. Bartlett, M. A. Barton, I. Bartos, R. Bassiri, A. Basti, M. Bawaj, J. C. Bayley, A. C. Baylor, M. Bazzan, B. Bécsy, V. M. Bedakhale, M. Bejger, I. Belahcene, V. Benedetto, D. Beniwal, T. F. Bennett, J. D. Bentley, M. Benyaala, F. Bergamin, B. K. Berger, S. Bernuzzi, C. P. L. Berry, D. Bersanetti, A. Bertolini, J. Betzwieser, D. Beveridge, R. Bhandare, U. Bhardwaj, D. Bhattacharjee, S. Bhaumik, I. A. Bilenko, G. Billingsley, S. Bini, R. Birney, O. Birnholtz, S. Biscans, M. Bischì, S. Biscoveanu, A. Bisht, B. Biswas, M. Bitossi, M. A. Bizouard, J. K. Blackburn, C. D. Blair, D. G. Blair, R. M. Blair, F. Bobba, N. Bode, M. Boer, G. Bogaert, M. Boldrini, L. D. Bonavena, F. Bondu, E. Bonilla, R. Bonnand, P. Booker, B. A. Boom, R. Bork, V. Boschi, N. Bose, S. Bose, V. Bossilkov, V. Boudart, Y. Bouffanais, A. Bozzi, C. Bradaschia, P. R. Brady, A. Bramley, A. Branch, M. Branchesi, J. Brandt, J. E. Brau, M. Breschi, T. Briant, J. H. Briggs, A. Brillet, M. Brinkmann, P. Brockill, A. F. Brooks, J. Brooks, D. D. Brown, S. Brunett, G. Bruno, R. Bruntz, J. Bryant, T. Bulik, H. J. Bulten, A. Buonanno, R. Busicchio, D. Buskulic, C. Buy, R. L. Byer, L. Cadonati, G. Cagnoli, C. Cahillane, J. C. Bustillo, J. D. Callaghan, T. A. Callister, E. Calloni, J. Cameron, J. B. Camp, M. Canepa, S. Canevarolo, M. Cannavacciuolo, K. C. Cannon, H. Cao, Z. Cao, E. Capocasa, E. Capote, and G. Carapella, Population of Merging Compact Binaries Inferred Using Gravitational Waves through GWTC-3, *Physical Review X* **13**, 011048 (2023), [arXiv:2111.03634 \[astro-ph.HE\]](#).

- [125] M. Favata, C. Kim, K. G. Arun, J. Kim, and H. W. Lee, Constraining the orbital eccentricity of inspiralling compact binary systems with Advanced LIGO, *Phys. Rev. D* **105**, 023003 (2022), [arXiv:2108.05861 \[gr-qc\]](#).
- [126] P. Saini, Resolving the eccentricity of stellar mass binary black holes with next generation ground-based gravitational wave detectors, *Mon. Not. Roy. Astron. Soc.* **528**, 833 (2024), [arXiv:2308.07565 \[astro-ph.HE\]](#).
- [127] I. Romero-Shaw, P. D. Lasky, and E. Thrane, Signs of Eccentricity in Two Gravitational-wave Signals May Indicate a Subpopulation of Dynamically Assembled Binary Black Holes, *ApJ* **921**, L31 (2021), [arXiv:2108.01284 \[astro-ph.HE\]](#).
- [128] P. Madau and M. Dickinson, Cosmic Star-Formation History, *ARA&A* **52**, 415 (2014), [arXiv:1403.0007 \[astro-ph.CO\]](#).
- [129] J. U. Jo, S. Youn, S. Kim, Y. Park, J. Hwang, J. H. Lee, and G. Kim, Star formation rate density across the cosmic time, *Ap&SS* **366**, 18 (2021).
- [130] J. Samsing, L. Zwick, P. Saini, D. J. D’Orazio, K. Hendriks, J. María Ezquiaga, R. K. L. Lo, L. Vujeva, G. D. Radev, and Y. Yu, Measuring the Transverse Velocity of Strongly Lensed Gravitational Wave Sources with Ground Based Detectors, [arXiv e-prints](#), [arXiv:2412.14159 \(2024\)](#), [arXiv:2412.14159 \[astro-ph.HE\]](#).
- [131] J. Samsing, L. Zwick, P. Saini, K. Hendriks, R. K. L. Lo, L. Vujeva, G. D. Radev, and Y. Yu, Constraining Proper Motion of Strongly Lensed Eccentric Binary Mergers using Doppler Triangulation, [arXiv e-prints](#), [arXiv:2501.12494 \(2025\)](#), [arXiv:2501.12494 \[astro-ph.HE\]](#).
- [132] L. Zwick and J. Samsing, The Proper Motion of Strongly Lensed Binary Neutron Star Mergers in LIGO/Virgo/Kagra can be Constrained by Measuring Doppler Induced Gravitational Wave Dephasing, [arXiv e-prints](#), [arXiv:2502.03547 \(2025\)](#), [arXiv:2502.03547 \[astro-ph.CO\]](#).
- [133] A. Tiwari, A. Vijaykumar, S. J. Kapadia, G. Fragione, and S. Chatterjee, Accelerated binary black holes in globular clusters: forecasts and detectability in the era of space-based gravitational-wave detectors, *MNRAS* **527**, 8586 (2024), [arXiv:2307.00930 \[astro-ph.HE\]](#).
- [134] L. Zwick, A. Derdzinski, M. Garg, P. R. Capelo, and L. Mayer, Dirty waveforms: multiband harmonic content of gas-embedded gravitational wave sources, *MNRAS* **511**, 6143 (2022), [arXiv:2110.09097 \[astro-ph.HE\]](#).
- [135] L. Zwick, P. R. Capelo, E. Bortolas, V. Vázquez-Aceves, L. Mayer, and P. Amaro-Seoane, Improved gravitational radiation time-scales II: Spin-orbit contributions and environmental perturbations, *MNRAS* **506**, 1007 (2021), [arXiv:2102.00015 \[astro-ph.GA\]](#).
- [136] L. Zwick, P. R. Capelo, E. Bortolas, V. Vázquez-Aceves, L. Mayer, and P. Amaro-Seoane, Improved gravitational radiation time-scales II: Spin-orbit contributions and environmental perturbations, *MNRAS* **506**, 1007 (2021), [arXiv:2102.00015 \[astro-ph.GA\]](#).
- [137] M. L. Katz, A. J. K. Chua, L. Speri, N. Warburton, and S. A. Hughes, Fast extreme-mass-ratio-inspiral waveforms: New tools for millihertz gravitational-wave data analysis, *Phys. Rev. D* **104**, 064047 (2021), [arXiv:2104.04582 \[gr-qc\]](#).
- [138] W.-B. Han, S.-C. Yang, H. Tagawa, Y. Jiang, P. Shen, Q. Yun, C. Zhang, and X.-Y. Zhong, Indication for a compact object next to a LIGO-Virgo binary black hole merger, [arXiv e-prints](#), [arXiv:2401.01743 \(2024\)](#), [arXiv:2401.01743 \[astro-ph.HE\]](#).
- [139] R. Abbott and et al., GW190814: Gravitational Waves from the Coalescence of a 23 Solar Mass Black Hole with a 2.6 Solar Mass Compact Object, *ApJ* **896**, L44 (2020), [arXiv:2006.12611 \[astro-ph.HE\]](#).
- [140] A. S. Hamers, An Improved Numerical Fit to the Peak Harmonic Gravitational Wave Frequency Emitted by an Eccentric Binary, *Research Notes of the American Astronomical Society* **5**, 275 (2021), [arXiv:2111.08033 \[gr-qc\]](#).
- [141] H. von Zeipel, Sur l’application des séries de M. Lindstedt à l’étude du mouvement des comètes périodiques, *Astronomische Nachrichten* **183**, 345 (1910).
- [142] Y. Kozai, Secular perturbations of asteroids with high inclination and eccentricity, *AJ* **67**, 591 (1962).
- [143] M. L. Lidov, The evolution of orbits of artificial satellites of planets under the action of gravitational perturbations of external bodies, *Planet. Space Sci.* **9**, 719 (1962).
- [144] F. Antonini, S. Chatterjee, C. L. Rodriguez, M. Morscher, B. Pattabiraman, V. Kalogera, and F. A. Rasio, Black Hole Mergers and Blue Stragglers from Hierarchical Triples Formed in Globular Clusters, *Astrophys. J.* **816**, 65 (2016), [arXiv:1509.05080 \[astro-ph.GA\]](#).
- [145] F. Antonini, S. Toonen, and A. S. Hamers, Binary Black Hole Mergers from Field Triples: Properties, Rates, and the Impact of Stellar Evolution, *Astrophys. J.* **841**, 77 (2017), [arXiv:1703.06614 \[astro-ph.GA\]](#).
- [146] K. Silsbee and S. Tremaine, Lidov-Kozai Cycles with Gravitational Radiation: Merging Black Holes in Isolated Triple Systems, *Astrophys. J.* **836**, 39 (2017), [arXiv:1608.07642 \[astro-ph.HE\]](#).
- [147] S. Toonen, H. B. Perets, and A. S. Hamers, Rate of WD-WD head-on collisions in isolated triples is too low to explain standard type Ia supernovae, *A&A* **610**, A22 (2018), [arXiv:1709.00422 \[astro-ph.HE\]](#).
- [148] C. L. Rodriguez and F. Antonini, A Triple Origin for the Heavy and Low-spin Binary Black Holes Detected by LIGO/VIRGO, *Astrophys. J.* **863**, 7 (2018), [arXiv:1805.08212 \[astro-ph.HE\]](#).
- [149] A. Vigna-Gómez, S. Toonen, E. Ramirez-Ruiz, N. W. C. Leigh, J. Riley, and C.-J. Haster, Massive Stellar Triples Leading to Sequential Binary Black Hole Mergers in the Field, *ApJ* **907**, L19 (2021), [arXiv:2010.13669 \[astro-ph.HE\]](#).
- [150] M. A. S. Martinez, G. Fragione, K. Kremer, S. Chatterjee, C. L. Rodriguez, J. Samsing, C. S. Ye, N. C. Weatherford, M. Zevin, S. Naoz, and F. A. Rasio, Black Hole Mergers from Hierarchical Triples in Dense Star Clusters, *Astrophys. J.* **903**, 67 (2020), [arXiv:2009.08468 \[astro-ph.GA\]](#).
- [151] M. Arca Sedda, G. Li, and B. Kocsis, Order in the chaos. Eccentric black hole binary mergers in triples formed via strong binary-binary scatterings, *A&A* **650**, A189 (2021), [arXiv:1805.06458 \[astro-ph.HE\]](#).
- [152] C. M. Will, Post-Newtonian effects in N-body dynamics: conserved quantities in hierarchical triple systems, *Classical and Quantum Gravity* **31**, 244001 (2014), [arXiv:1404.7724 \[astro-ph.GA\]](#).
- [153] A. Antoni, M. MacLeod, and E. Ramirez-Ruiz, The Evolution of Binaries in a Gaseous Medium:

- Three-dimensional Simulations of Binary Bondi-Hoyle-Lyttleton Accretion, *Astrophys. J.* **884**, 22 (2019), [arXiv:1901.07572 \[astro-ph.HE\]](#).
- [154] R. Li and D. Lai, Hydrodynamical evolution of black-hole binaries embedded in AGN discs, *MNRAS* **517**, 1602 (2022), [arXiv:2202.07633 \[astro-ph.HE\]](#).
- [155] A. M. Dempsey, H. Li, B. Mishra, and S. Li, Contracting and Expanding Binary Black Holes in 3D Low-mass AGN Disks: The Importance of Separation, *Astrophys. J.* **940**, 155 (2022), [arXiv:2203.06534 \[astro-ph.HE\]](#).
- [156] C. Rowan, T. Boekholt, B. Kocsis, and Z. Haiman, Black Hole Binary Formation in AGN Disks: From Isolation to Merger, *arXiv e-prints*, [arXiv:2212.06133 \(2022\)](#), [arXiv:2212.06133 \[astro-ph.GA\]](#).
- [157] H. Whitehead, C. Rowan, T. Boekholt, and B. Kocsis, Gas Assisted Binary Black Hole Formation in AGN Disks, *arXiv e-prints*, [arXiv:2309.11561 \(2023\)](#), [arXiv:2309.11561 \[astro-ph.GA\]](#).
- [158] A. J. Dittmann, A. M. Dempsey, and H. Li, The Evolution of Inclined Binary Black Holes in the Disks of Active Galactic Nuclei, *Astrophys. J.* **964**, 61 (2024), [arXiv:2310.03832 \[astro-ph.HE\]](#).
- [159] A. J. Dittmann, A. M. Dempsey, and H. Li, The Evolution of Inclined Binary Black Holes in the Disks of Active Galactic Nuclei, *arXiv e-prints*, [arXiv:2310.03832 \(2023\)](#), [arXiv:2310.03832 \[astro-ph.HE\]](#).
- [160] P. Goldreich and S. Tremaine, Disk-satellite interactions., *Astrophys. J.* **241**, 425 (1980).
- [161] D. N. C. Lin and J. Papaloizou, On the Tidal Interaction between Protoplanets and the Protoplanetary Disk. III. Orbital Migration of Protoplanets, *Astrophys. J.* **309**, 846 (1986).
- [162] C. Rowan, H. Whitehead, T. Boekholt, B. Kocsis, and Z. Haiman, Black hole binaries in AGN accretion discs - II. Gas effects on black hole satellite scatterings, *MNRAS* **527**, 10448 (2024), [arXiv:2309.14433 \[astro-ph.HE\]](#).
- [163] Y.-P. Li, A. M. Dempsey, S. Li, H. Li, and J. Li, Orbital Evolution of Binary Black Holes in Active Galactic Nucleus Disks: A Disk Channel for Binary Black Hole Mergers?, *Astrophys. J.* **911**, 124 (2021), [arXiv:2101.09406 \[astro-ph.HE\]](#).
- [164] H. Tagawa, Z. Haiman, and B. Kocsis, Formation and Evolution of Compact-object Binaries in AGN Disks, *Astrophys. J.* **898**, 25 (2020), [arXiv:1912.08218 \[astro-ph.GA\]](#).
- [165] C. Rowan, H. Whitehead, and B. Kocsis, Black Hole Merger Rates in AGN: contribution from gas-captured binaries, *arXiv e-prints*, [arXiv:2412.12086 \(2024\)](#), [arXiv:2412.12086 \[astro-ph.HE\]](#).
- [166] C. Baruteau, J. Cuadra, and D. N. C. Lin, BINARIES MIGRATING IN A GASEOUS DISK: WHERE ARE THE GALACTIC CENTER BINARIES?, *Astrophys. J.* **726**, 28 (2010).
- [167] R. Li and D. Lai, Hydrodynamical evolution of black-hole binaries embedded in AGN discs - III. The effects of viscosity, *MNRAS* **529**, 348 (2024), [arXiv:2303.12207 \[astro-ph.HE\]](#).
- [168] R. S. Beckmann, A. Slyz, and J. Devriendt, Bondi or not Bondi: the impact of resolution on accretion and drag force modelling for supermassive black holes, *MNRAS* **478**, 995 (2018), [arXiv:1803.03014 \[astro-ph.HE\]](#).
- [169] G. Fabj, S. S. Nasim, F. Caban, K. E. S. Ford, B. McKernan, and J. M. Bellovary, Aligning nuclear cluster or- bits with an active galactic nucleus accretion disc, *MNRAS* **499**, 2608 (2020), [arXiv:2006.11229 \[astro-ph.GA\]](#).
- [170] H. Bondi, On spherically symmetrical accretion, *MNRAS* **112**, 195 (1952).
- [171] L. Zwick, P. R. Capelo, E. Bortolas, V. Vázquez-Aceves, L. Mayer, and P. Amaro-Seoane, Improved gravitational radiation time-scales II: Spin-orbit contributions and environmental perturbations, *MNRAS* **506**, 1007 (2021), [arXiv:2102.00015 \[astro-ph.GA\]](#).
- [172] E. C. Ostriker, Dynamical Friction in a Gaseous Medium, *Astrophys. J.* **513**, 252 (1999), [arXiv:astro-ph/9810324 \[astro-ph\]](#).
- [173] C. Dyson, T. F. M. Spieksma, R. Brito, M. van de Meent, and S. Dolan, Environmental effects in extreme mass ratio inspirals: perturbations to the environment in Kerr, *arXiv e-prints*, [arXiv:2501.09806 \(2025\)](#), [arXiv:2501.09806 \[gr-qc\]](#).
- [174] D. Lai and D. J. Muñoz, Circumbinary Accretion: From Binary Stars to Massive Binary Black Holes, *arXiv e-prints*, [arXiv:2211.00028 \(2022\)](#), [arXiv:2211.00028 \[astro-ph.HE\]](#).
- [175] N. I. Shakura and R. A. Sunyaev, Black holes in binary systems. Observational appearance., *A&A* **24**, 337 (1973).
- [176] C. Tiede, J. Zrake, A. MacFadyen, and Z. Haiman, Gas-driven Inspiral of Binaries in Thin Accretion Disks, *Astrophys. J.* **900**, 43 (2020), [arXiv:2005.09555 \[astro-ph.GA\]](#).
- [177] P. J. Armitage and P. Natarajan, Accretion during the Merger of Supermassive Black Holes, *ApJ* **567**, L9 (2002), [arXiv:astro-ph/0201318 \[astro-ph\]](#).
- [178] A. J. Dittmann, G. Ryan, and M. C. Miller, The Decoupling of Binaries from Their Circumbinary Disks, *ApJ* **949**, L30 (2023), [arXiv:2303.16204 \[astro-ph.HE\]](#).
- [179] D. O’Neill, C. Tiede, D. J. D’Orazio, Z. Haiman, and A. MacFadyen, Gravitational Wave Decoupling in Retrograde Circumbinary Disks, *arXiv e-prints*, [arXiv:2501.11679 \(2025\)](#), [arXiv:2501.11679 \[astro-ph.HE\]](#).
- [180] L. Ennoggi, M. Campanelli, Y. Zlochower, S. C. Noble, J. Krolik, F. Cattorini, J. V. Kalinani, V. Mewes, M. Chabanov, L. Ji, and M. C. de Simone, Relativistic Gas Accretion onto Supermassive Black Hole Binaries from Inspiral through Merger, *arXiv e-prints*, [arXiv:2502.06389 \(2025\)](#), [arXiv:2502.06389 \[astro-ph.HE\]](#).
- [181] M. Mapelli, Formation Channels of Single and Binary Stellar-Mass Black Holes, in *Handbook of Gravitational Wave Astronomy* (2021) p. 4.
- [182] H. Wang, A. P. Stephan, S. Naoz, B.-M. Hoang, and K. Breivik, Gravitational-wave Signatures from Compact Object Binaries in the Galactic Center, *Astrophys. J.* **917**, 76 (2021), [arXiv:2010.15841 \[astro-ph.HE\]](#).
- [183] C. Rowan, H. Whitehead, G. Fabj, P. Saini, B. Kocsis, M. Pessah, and J. Samsing, Prompt gravitational-wave mergers aided by gas in Active Galactic Nuclei: The hydrodynamics of binary-single black hole scatterings, *arXiv e-prints*, [arXiv:2501.09017 \(2025\)](#), [arXiv:2501.09017 \[astro-ph.GA\]](#).
- [184] J. M. Bellovary, M.-M. Mac Low, B. McKernan, and K. E. S. Ford, Migration Traps in Disks around Supermassive Black Holes, *ApJ* **819**, L17 (2016), [arXiv:1511.00005 \[astro-ph.GA\]](#).

- [185] F. Camilloni, G. Grignani, T. Harmark, M. Orselli, and D. Pica, Binary mergers in strong gravity background of Kerr black hole, [arXiv e-prints](#), [arXiv:2310.06894 \(2023\)](#), [arXiv:2310.06894 \[gr-qc\]](#).
- [186] E. Sirko and J. Goodman, Spectral energy distributions of marginally self-gravitating quasi-stellar object discs, *MNRAS* **341**, 501 (2003), [arXiv:astro-ph/0209469 \[astro-ph\]](#).
- [187] J. Goodman, Self-gravity and quasi-stellar object discs, *MNRAS* **339**, 937 (2003), [astro-ph/0201001](#).
- [188] J. E. Greene and L. C. Ho, The Mass Function of Active Black Holes in the Local Universe, *Astrophys. J.* **667**, 131 (2007).